Supporting Information

Activation mechanism of the G protein-coupled sweet receptor heterodimer with sweeteners and allosteric agonists

Soo-Kyung Kim,[*†] *Yalu Chen,*[†] *Ravinder Abrol,*[†,‡] *William A. Goddard III,*[*†] and Brian Guthrie[§]

[†]Materials and Process Simulation Center (MC 139-74), California Institute of Technology,
1200 E. California Blvd., Pasadena, CA 91125;

[‡]Current address, Departments of Chemistry and Biochemistry, California State University, Northridge, CA 91330;

[§]Cargill Global Food Research, 2301 Crosby Road, Wayzata, MN 55391

*** CORRESPONDING AUTHOR**

Prof. William A. Goddard III

California Institute of Technology MC 139-74, 1200 E. California Blvd., Pasadena, CA 91125; phone: 1-626-395-2731, e-mail: wag@wag.caltech.edu

Dr. Soo-Kyung Kim

phone: 1-626-395-2724, e-mail: skkim@wag.caltech.edu

RESULTS

Structures for Allosteric ligand bound at the TMD of all three TAS1Rs

As described in the METHODS section, the DarwinDock procedure (1) involves sampling ~50,000 poses for each of ~10 diverse ligand conformations from which, we select finally two energetically favorable binding poses based on two scoring methods:

- UCav E: unified cavity energy for which we consider that interactions of the best 100 poses with the union of all residues involve in their separate binding sites (providing a uniform comparison)
- BE: snap binding energy considering all interactions of ligand with protein

As a first validation of the predicted structures for the 7 helix TMD, we used DarwinDock to predict the binding site for the allosteric ligands to each TAS1R TMD in Table S10. Here we find,

- S819 [1-((1H-pyrrol-2-yl)methyl)-3-(4-isopropoxyphenyl)thiourea] is a sweet compound that interacts with the TAS1R2 TMD.(2) and
- Lactisole is a competitive inhibitor of the sweet taste receptor that binds to TAS1R3 TMD.(3, 4)

These structures were further relaxed through annealing. To check the stability of the binding site of these allosteric ligands, we inserted the predicted complexes into an explicit lipid (POPC) and water and carried out 10 ns of MD in physiological salt concentration at 310 K. Figure S2 shows the binding site of

- S807 at the TMD of TAS1R1,
- S819 at the TMD of TAS1R2, and
- lactisole at the TMD of TAS1R3.

GEnSeMBLE predictions of the structures for the 7-helix TMD bundles for all three TASRs of family 1

We sampled 13 trillion combinations of rotations and tilts of the 7 transmembrane helices that we expect to include all plausible packings of the 7 helices into a bundle. Then we used the BiHelix mean field analysis of all pair-wise interactions of these 7 helices to estimate the energy for all 13 trillion packings. Based on this mean field estimate we selected the best 2000, built them into 7-helix bundles, and reevaluated the energy considering interactions of all seven helices with each other. Then we selected the most stable 25 for further analysis.

For TAS1R1 we selected the 3 configurations (t1, t7, t8) with an asterisk from Table S7. During the MD of TAS1R1 (t8), the HB between N735 (5.47) and CO in S807 at the binding site of the TMD is found to be stable (Figure S2A). Also the TAS1R1 MD maintains the salt-bridge interactions in TMs 3-6-7 among R652 (3.46), E758 (6.33), and K811 (7.53). For TAS1R2 we selected the 3 configurations (t1, t9, t19) with an asterisk from Table S8. For TAS1R3 we selected the 3 configurations (t1, t15, t22) with an asterisk from Table S9. The allosteric ligands bind to the TMD of TAS1Rs (S807 at TAS1R1 t8, S819 at TAS1R2 t19, lactisole at TAS1R3 t15), with the interactions stable in the MD studies.

For TAS1R2, Table S8 shows that 22 out of the top 25 TMD in the ensemble of structures for TAS1R2 contained salt-bridges between the conserved R3.46 and E6.33 at the intracellular interface, coupling TM 3-6, as observed in X-ray structures of inactive Class C GPCR. We

observed hydrogen bonding (HB) networks involving TMs 2-3, TMs 3-4-5, (Q4.53-N5.47) and TMs 6-7 that we also found for TAS1R1. But we found an additional salt-bridge between K4.53-D5.47 in the upper TMD of TAS1R2.

For TAS1R1, Table S7 shows that 21 to 24 of the top 25 have close TM3-TM6 interactions at the intracellular surface while 3 out of the 25 do not show this interaction. Based on our previous studies we expect that structure #22 lacking the TM 3-6 interactions may correspond to an active conformation. We also observed HB networks involving TMs 2-3, TMs 3-4-5, (Q4.53-N5.47) and TMs 6-7 in TAS1R1.

The interactions within the TMD for TAS1R1 and TAS1R2 are both consistent with them having an un-activated conformation.

For TAS1R3, the conserved R3.46-E6.33 forming salt bridges in TAS1R1 and TAS1R2 are replaced by Q3.46 and R6.33 in TAS1R3, leading only to HBs in Table S9. Thus we obtain a 3-6 HB not a salt bridge. As a result, there is no strong 3-6 coupling for 20 of the 25 low lying structures. Instead we find a TM 3-4 salt-bridge between E3.49 and R4.40 for 24 of the 25 structures. Thus TAS1R3 is stabilized in what appears as an activated form with few inter-helical couplings. We find that 19 cases have clearly broken TM 3-6 interactions, so that these 19 structures are candidate active conformations. TAS1R3 has the fewest inter-helical constraints among the three TAS1Rs.

The full TAS1R2/TAS1R3 heterodimer sweet taste receptors

1) Building the structure of the full TAS1R2/TAS1R3 heterodimer

The key observations are:

- The dimer interface of the OPRK is formed through contacts of TM1, TM2, and helix8 (H8), denoted at TM12H8/TM12H8, leading to ~1,100 $Å^2$ buried surface area.
- Two different interfaces were found for the crystal structure of the OPRM; TM56/TM56 interface with 1492 $Å^2$ buried surface area and TM12H8/TM12H8 interface with 615 $Å^2$ buried surface area. This might indicate a structural basis for the existence of higher-order oligomers (5) or it might just be an artifact of the crystallization in the surfactant. OPRM dimer had interactions between TM56/TM56 for each TMD (Fig. S3 center).
- The β_1AR receptor also displayed a TM45/TM45 interface with 900 $Å^2$ buried surface area and a TM12H8/ TM12H8 interface with 1700 $Å^2$ buried surface area.(6)

These interfaces provided reasonable starting dimer interface structures for our activation studies. For the TM12 dimer, the distance between the start of TM1 for the two TMD bundles is ~20 Å, which is too short to connect the VFD2 and VFD3 domain of the VFD dimer. Since the VFDs would need to be rotated 90˚ to interact with each other as shown in Fig. S3, we consider Model 12 as physiologically unrealistic.

The TM45/TM45 interface has now been seen in several GPCR structures. For Class C GPCRs biophysical measurements shown that this TM45/TM45 interface is associated with the inactive or resting state (R). In contrast the interface coupling TM6/TM6 on both TMD has been associated with the fully active state (A).(7, 8)

Based on the models, we constructed a heterodimer (Fig. S3).

OPRM dimer with interaction between TM5/6 for each TMD (Fig. S3 center). We considered this to Model 12, the distance between the start of TM1 for the two TMD bundles is ~20 Å, which is too short to connect the VFD2 and VFD3 domain of the VFD dimer. Since the VFDs would need

to be rotated 90˚ to interact with each other as shown in Fig. S3, we consider Model 12 as physiologically unrealistic.

2) MD of the 45oo predicted structure of the TAS1R2/TAS1R3 heterodimer

We also carried out 10 ns of MD for the Model 45 ooR apo form with TM45/TM45 interface in an explicit lipid bilayer using the same protocol as for the systems described above. We found that the initial structure was stable over the course of the simulation with no change in the TMD or VFD interfacial configuration. The TAS1R2 and TAS1R3 VFDs remained held tightly together by two salt bridge interactions [E118(R2):K111(R3) and D119(R2):R123(R3)] and a strong polar interaction between Q109(R2) and the backbone NH groups of three residues (K119, A120, G121) forming a sharp turn in TAS1R3. The two CRD domains exhibit a hydrophobic interaction [L521(R2):T539+F540(R3)]. The TM domains of TAS1R2 and TAS1R3 showed stable salt bridge interaction R674(R2):E663(R3) across the two ICL2 loops. In addition, The TM4/5 interface was held tightly in place by two groups of hydrophobic interactions:

- TAS1R2[TM3(F653+V656)+TM5(L737+V741+F745+M748)]:TAS1R3[TM4(L676+W680+L687)], and
- TAS1R2[TM4(L688+F684+V680):TAS1R3[TM3(F659+V660)+TM5(T739+L743)].

Fig. S10 shows these interactions, which are the main chemical couplings keeping the sweet receptor inactive. We see that they span the whole receptor from the VFD to the CRD, to the TMD. Many of these interactions would need to be broken during receptor activation as the TMD interface switches from the TM45/TM45 interface to the TM56/TM56 interface while the VFD dimer switches from the ooR to the coA conformation, as suggested by many biophysical observations on mGluR.(7, 9-11)

MD of the TAS1R2/TAS1R3 heterodimer bound with Stev.

To check the stability of the predicted binding site of Stev, we inserted the predicted VFD heterodimer complex into a periodic box with explicit and water at physiological salt concentration (103,993 total atoms) and carried out 12 ns of MD at 310 K. As shown in Fig S7, the Stev binding site shows overall stability through all 12 ns MD, with some minor changes in the HBs at the binding site of the flexible hydroxyl group of the glucose ring. We find that the strong interactions at D142 and E302, which are critical residues for sucrose activity, were maintained during the MD (Fig. S5A). We observed new HB interactions from N70 with the OH group (Fig. S5B & Table S11). In addition, we found additional water-mediated interactions: (a) At 3.3 ns one water inserted into the binding cavity and (b) at 5.5 ns another water molecule formed a water mediated HB (Fig. S5C). We also observed that the intramolecular HBs in Stev are maintained (Fig. S5D & Fig. S6).

To select the best binding pose from the 12 ns MD trajectory, we calculated the interaction energy between protein and ligands along the trajectory and selected the 6 snapshots in Fig. S7, with good interaction energies. Then we matched 4 known Stev analogues into the binding site to examine if these structures could explain experimental structure-activity relationship (SAR) of various Stev derivatives.(8) All 5 Stev derivatives show the important interactions displayed in orange at all 6 time steps, especially at D142 and E302, with additional interactions depending on the terminal sugar orientations/ conformations. In addition, we find no interactions of these Stev type molecules with the residues in purple that were established from mutational studies to not be important in activation. Fig. S8 displays the pharmacophore map at 6 different time steps.

The short MD simulations of MogV bound complex also support the stability of the MogV binding site. The predicted binding site of MogV with the TAS1R2/ TAS1R3 VFD heterodimer indicates that D278 stabilizes the conformation through interaction with K65. As in the Stev-bound complex, we also observed that the electrostatic interactions between K65 and D278 remain stable through the MD, stabilizing the conformation. We also find that R383 stabilizes the conformation through interaction with D307 at VFD2, favoring the closed conformation.

METHODS

1. Structure predictions for TAS1Rs

We used the GEnSeMBLE method(12) to generate the 3D structures for the ensemble TMD conformations of all TAS1Rs. GEnSeMBLE evaluates mean field energies for all the conformations sampled by varying the helix tilts and rotations (13 trillion). This leads to selection of ~25 low energy conformations to be used for binding to different ligands. This structure prediction methodology has been described previously,(12) but we summarize it here:

1.1 Homologize Helices: Since all TAS1Rs belongs to Class C GPCRs with 17.29~25.14% sequence identities in the TMD, we generated the homology helices using the X-ray structures of Class C GPCRs: human mGluR1 (PDB ID: 4OR2)(13) and mGluR5 (PDB ID: 4OO9).(14) We also used these two structures as the starting template for our complete sampling of rotations and tilts.

1.2 BiHelix: We sample all possible helix rotation combinations leading to $(12)^7$ ~ 35 million packings. Starting with the two templates, we find that the lowest energy conformations from BiHelix do not show rotation angle changes from the X-ray structure of the templates.

1.3 SuperBiHelix: In this step, helix tilt angles are added to helix rotations for rigorous conformational sampling in the membrane.(15) This leads to a sampling of ~13 trillion conformations. The top 25 structures by energy were selected for further use and analysis.

1.4 Loop generation: After optimizing the TM domains, we constructed the loops using homology to human mGluR1 (PDB ID: 4OR2)(13) for hTAS1R1/ 3 and human mGluR5 (PDB ID: 4OO9)(14) for hTAS1R2. The loops and the N/C terminus including helix 8 for each new structure were modeled through homology with the template structure, and then relaxed through 10 cycles of simulated annealing with fixed TM domains between 50 K and 600 K each for 100 ps per cycle. We then minimized the whole structures up to 1000 CG steps but terminating when the RMS forces are below 0.5 kcal/mol-A. The disulfide bridges between $C630^{3.25}$ and C720 in TAS1R2, and between $C633^{3.25}$ and C722 in TAS1R3 (conserved among most GPCRs) were constructed by homology. The lowest energy loops were used to generate the full structure of the TMD.

1.5 VFD and CRD generation: X-ray structures of the VFD in Class C GPCRs suggest 5 possible dimer conformations. Agonist induced transformations between these structures plays a role in receptor activation of Class C GPCR dimers. We constructed the "oo" resting state based on the rat metabotropic glutamate receptor 1 (mGluR1) structure (PDBid: 1ewt).(16) We based the "co" and "cc" active states apo structures on homology modeling of rat mGluR1 (PDBid: 1ewk)(16) and human mGluR5 (PDBid: 3lmk) respectively. The rat mGluR3 was used as a template for modeling the CRD domain. The homology modeling was performed with the Swiss-Model server(17) using the above mentioned crystal structure templates as input. The disulfide bridges in the N-terminal domain of TAS1R2 were constructed by homology:

C59-C102, C359-C363, C405-C410 in the VFD,

C495-C514, C499-C517, C520-C535, C538-C551 in the CRD, and

C233-C513 between the VFD and CRD.

The disulfide bridges in the N-terminal domain of TAS1R3 were constructed by homology:

C62-C103, C351-C370, C373-C375, C410-C415 in the VFD,

C499-C518, C503-C521, C524-C538, C541-C554 in the CRD, and

C236-C517 between the VFD and CRD.

1.6 Heterodimer generation: To construct the heterodimer with TMD interfaces between TAS1R2 and TAS1R3, we used recent crystal structures of Class A μ opioid receptor (OPRM),(5) κ opioid receptor (OPRK),(18) and β_1 adrenergic receptor (β_1AR).(6) The crystal structures of OPRM (PDB: 4DKL), OPRK (PDB: 4DJH), and β_1AR (PDB: 4GPO) were used as a template for the structure alignment to generate a parallel, symmetric dimer with symmetric dimeric interfaces. We aligned each monomer to the template using Protein Structure Alignment tool in the Maestro software.(19)

2. Predicting ligand binding sites

For each ligand multiple torsional conformations are used in DarwinDock (1) that iteratively generates ~50,000 poses in the putative binding regions. The amino acid sidechains in the binding site are optimized for each ligand pose, the resulting complex is neutralized, and its energy minimized as described earlier.(26) This procedure was followed for each of ligand conformations generated as follows. Starting from the minimized structure of the S807, S819, lactisole and the X-ray structures of sucrose and stevioside ligands, we performed conformational searches of Mixed torsional/ Low-mode sampling (1000 steps, 1000 steps per rotatable bond, 10 kcal/mol of energy window, 0.5 Å of RMSD) using the Maestro software.(19) The low energy conformations were re-minimized using the Dreiding force field (20) with some modifications in the HB interactions and clustered by 2.0 and 1.0 Å of RMSD in two steps. For docking, various low energy conformations for ligands were selected: 4 for S807, 8 for S819, 2 for lactisole, 3 for sucrose, and 9 for stevioside,

3. Full solvent MD

3.1 Allosteric ligands bound to the TMD of TAS1R1, TAS1R2, and TAS1R3: The predicted structures for the complexes:

S807-TAS1R1 (38,308 total atoms including 6,664 waters, 17 Na^+, 21 Cl^-),

S819-TAS1R2 (38,886 total atoms including 6,698 waters, 14 Na^+, 23 Cl^-), and

lactisole-TAS1R3 (38,130 total atoms including 6,700 waters, 17 Na^+, 21 Cl^-)

were inserted into a continuous infinite POPC lipid bilayer membrane with periodic boundary conditions while including full solvation with water at physiological salt concentration. We then carried out 10 ns MD at 300 K. In these calculations H641 (3.33) and H734 (5.44) in TAS1R3 were treated as a protonated His, HSP. The procedure here was identical to that in Kim. *et al*.(21)

3.2 Stevioside bound to the VFD of TAS1R2/TAS1R3 heterodimer: The predicted structure for stevioside bound to the VFD of TAS1R2/ TAS1R3 heterodimer (104,173 total atoms including 29,778 waters, 101 Na^+, 79 Cl^-) was inserted into a continuous infinite POPC lipid bilayer membrane with periodic boundary conditions while including full solvation with water in physiological salt concentration. We then carried out 12 ns MD at 300 K.

3.3 Stevioside and S819 bound the whole complex of TAS1R2/ TAS1R3 heterodimer: The DarwinDock predicted structure for stevioside and S819 bound to the whole complex of TAS1R2/ TAS1R3 heterodimer was inserted into a continuous infinite lipid bilayer POPC membrane with periodic boundary conditions while including full solvation with water in physiological salt

concentration (177,398 total atoms including 40,030 waters, 117 Na^+, 107 Cl^-). We then carried out 30 ns MD at 300 K.

The following disulfide bridges in TAS1R2 were constrained:

C59-C102, C359-C363, C405-C410 in the VFD,

C495-C514, C499-C517, C520-C535, C538-C551 in CRD,

C233-C513 between VFD and CRD, and

$C630^{3.25}$-C720 between TMDTMD and EC2.

The disulfide bridges in TAS1R3 were also constrained:

C62-C103, C351-C370, C373-C375, C410-C415 in VFD,

C499-C518, C503-C521, C524-C538, C541-C554 in CRD,

C236-C517 between VFD and CRD, and

$C633^{3.25}$and C722 between TMDTMD and EC2.

The POPC lipid available in VMD is used to insert the protein into a lipid-water box, lipids within 1 Å of protein and waters within 2 Å of the protein are removed.

For the particle mesh Ewald (PME) in the electrostatics calculation,(22) the charge of system was balanced through replacing waters into Na^+ and Cl^- ions. Here we used AMBER tool *tleap* to place the ions at their best electrostatic potions. After inserting the 7 helix bundle including loops into the box containing the periodic POPC membrane, water, and ions, we fixed the protein and minimized the lipid, water, ion atoms for 1,000 steps, and then equilibrated with NPT dynamics for 500 ps while continuing to keep the protein fixed. This allows the lipid and water to readjust to the protein. Then we minimized the full system for 1,000 steps and then performed NPT dynamics. This predicted structure was then equilibrated at 300 K using the NAMD 2.9 (NAnoscale Molecular Dynamics) program.(23) We used the CHARMM22 force field parameters for the protein, the TIP3 model for water,(24) and the CHARMM27 force field parameters for the lipids.(25)

Table S1. Top 10 structures for TAS1R1 taste receptor from BiHelix ranked by the average rank of the charged total (CTot), neutralized total (Ntot), charged interhelical (CIH), and neutralized interhelical (NIH) energy. The eta, η, (rotation) angles and the backbone RMSD (Å) with respect to the starting conformation were displayed. The homology templates were used with human metabotropic glutamate receptor (mGluR), mGluR 1 and mGluR5. Three structures in grey were optimized with SuperBihelix.

#	H1	H2	H3	H4	H5	H6	H7	Template	CIH	CTot	NIH	NTot	RMSD
1	-120	-90	0	0	0	0	60	mGluR1	-379.15	130.90	-391.42	35.52	2.15
2	-90	-90	0	0	0	0	60	mGluR1	-374.67	134.12	-392.24	20.54	2.00
3	90	0	0	0	0	0	0	mGluR1	-381.39	100.42	-383.90	2.99	1.18
4	-30	-90	0	0	0	0	30	mGluR1	-373.98	161.36	-399.08	45.69	1.38
4	0	-90	0	0	0	0	60	mGluR1	-374.16	149.17	-393.13	49.23	1.64
5	180	-90	0	0	0	0	60	mGluR1	-366.74	149.62	-386.17	45.96	2.29
5	-120	-90	0	0	0	0	30	mGluR1	-371.14	167.71	-399.47	49.28	1.91
6	90	0	0	30	0	0	0	mGluR1	-371.50	139.05	-374.15	39.53	1.26
7	-150	-90	0	0	0	0	0	mGluR1	-362.88	170.20	-382.15	47.63	1.94
8	-120	-90	0	60	0	0	60	mGluR1	-362.19	147.09	-376.98	47.80	2.32
9	0	0	0	0	0	0	0	mGluR1	-372.59	143.88	-371.36	41.50	0.35
10	0	0	0	0	0	0	0	mGluR5	-377.57	197.18	-405.70	59.03	0.35

Table S2. Top 10 structures for TAS1R2 taste receptor from BiHelix ranked by the average rank of the charged total (CTot), neutralized total (Ntot), charged interhelical (CIH), and neutralized interhelical (NIH) energy. The eta, η, (rotation) angles and the backbone RMSD (Å) with respect to the starting conformation were displayed. The homology templates were used with human metabotropic glutamate receptor (mGluR), mGluR 1 and mGluR5. Top 1 structure in grey was optimized with SuperBihelix.

#	H1	H2	H3	H4	H5	H6	H7	Template	CIH	CTot	NIH	NTot	RMSD
1	0	0	0	30	0	0	0	mGluR5	-442.27	133.23	-395.57	132.87	0.51
2	0	0	0	90	0	0	0	mGluR5	-411.19	149.76	-378.14	120.76	1.20
3	30	0	0	90	0	0	0	mGluR5	-412.71	175.70	-377.90	136.37	1.27
4	0	0	0	0	-30	0	0	mGluR5	-420.31	153.89	-369.85	162.19	0.53
5	0	0	0	150	0	0	0	mGluR5	-407.88	177.59	-380.46	141.34	1.62
6	30	0	0	0	0	0	0	mGluR5	-411.29	198.52	-361.49	173.87	0.49
6	0	0	0	120	0	0	0	mGluR5	-395.01	179.51	-366.63	127.81	1.46
7	-30	0	0	90	0	0	0	mGluR5	-391.43	165.19	-364.32	132.55	1.27
8	0	0	0	30	0	0	0	mGluR1	-405.52	208.19	-367.91	198.21	0.53
9	0	0	0	0	0	0	0	mGluR5	-391.24	151.38	-354.20	134.12	0.00
10	-30	0	0	0	0	0	0	mGluR5	-396.81	167.83	-353.45	165.24	0.50

Table S3. Top 12 structures for TAS1R3 taste receptor from BiHelix ranked by the average rank of the charged total (CTot), neutralized total (Ntot), charged interhelical (CIH), and neutralized interhelical (NIH) energy. The eta, η, (rotation) angles and the backbone RMSD (Å) with respect to the starting conformation were displayed. The homology templates were used with human metabotropic glutamate receptor (mGluR), mGluR 1 and mGluR5. Three structures in grey were optimized with SuperBihelix.

#	H1	H2	H3	H4	H5	H6	H7	Template	CIH	CTot	NIH	NTot	RMSD
1	0	0	0	-150	0	0	0	mGluR1	-569.97	-29.68	-386.13	-16.80	1.71
2	0	0	0	150	0	-90	0	mGluR1	-556.26	1.20	-385.68	-3.59	2.07
3	0	0	0	120	0	0	0	mGluR1	-540.26	-12.68	-361.45	-19.77	1.54
4	0	0	0	150	0	0	0	mGluR1	-533.85	-15.03	-361.96	-24.42	1.71
5	0	0	0	180	0	0	0	mGluR1	-537.03	-40.68	-354.65	-28.81	1.76
6	0	0	0	180	0	0	0	mGluR5	-539.19	29.74	-380.49	-0.58	1.66
7	30	0	0	-150	0	0	0	mGluR1	-540.92	20.55	-368.61	25.26	1.76
8	0	0	0	-150	0	-90	0	mGluR1	-561.56	24.93	-371.43	28.53	2.07
9	30	0	0	150	0	0	0	mGluR1	-525.47	21.51	-363.32	7.13	1.76
10	0	0	0	0	0	0	0	mGluR1	-509.04	-30.81	-382.55	-55.54	0.35
11	0	0	0	180	0	-90	0	mGluR1	-523.93	1.50	-356.82	4.76	2.12
12	0	0	0	30	0	-90	0	mGluR1	-508.45	14.17	-391.12	-22.49	1.30

Table S4. Top 25 structures for TAS1R1 taste receptor from SuperBihelix ranked by the average rank of the charged total (CTot), neutralized total (Ntot), charged interhelical (CIH), and neutralized interhelical (NIH) energy. Theta, θ, (tilt), phi, ϕ, (sweep), eta, η, (rotation) angles and the backbone RMSD (Å) with respect to the starting conformation. Top 1,2,10,13,23 structures are from mGluR1-top1, Top 3-7,9,11,12,14-22,24 structures are from mGluR1-top3, and Top 8, 24 structures are from mGluR5-top10 in BiHelix runs.

#	θ (tilt)							ϕ (sweep)							η (rotation)							CIH	CTot	NIH	NTot	RMSD
	H1	H2	H3	H4	H5	H6	H7	H1	H2	H3	H4	H5	H6	H7	H1	H2	H3	H4	H5	H6	H7					
1	0	0	0	0	0	0	0	0	0	0	0	0	0	0	0	0	0	0	0	0	0	-394.5	125.7	-406.3	27.9	0.0
2	0	0	0	0	0	0	0	0	0	0	0	-30	30	0	0	0	0	0	0	0	-30	-392.9	137.5	-403.8	25.4	1.0
3	0	0	0	0	0	0	0	0	0	0	0	0	0	0	0	0	0	0	0	0	0	-396.4	82.8	-383.9	-7.5	0.4
4	0	0	0	0	0	0	0	0	0	0	0	-30	30	0	0	0	0	0	0	0	0	-414.0	142.5	-396.1	50.1	0.8
5	0	0	0	0	0	0	0	0	0	0	30	0	0	0	0	0	0	0	0	0	0	-408.5	135.9	-377.3	50.8	0.4
6	0	0	0	0	0	0	0	0	0	0	-60	-30	30	0	0	0	0	0	0	0	0	-398.1	144.7	-386.6	54.9	0.8
7	10	0	0	0	0	0	-10	0	0	0	30	-30	30	0	0	0	0	0	0	0	0	-383.7	138.2	-377.6	41.8	1.3
8	10	0	0	0	0	0	0	0	0	0	30	0	-30	0	0	0	0	0	0	0	0	-387.3	163.2	-399.5	52.9	0.9
9	0	0	0	0	0	0	0	0	0	0	30	-30	30	0	0	0	0	0	0	0	0	-408.8	147.2	-380.5	58.1	0.8
10	0	0	0	0	0	0	0	0	0	0	30	-30	30	0	0	0	0	0	0	0	0	-390.5	150.9	-379.2	54.2	0.8
11	0	0	0	0	0	0	0	0	0	0	-30	-30	30	0	0	0	0	0	0	0	0	-393.2	146.0	-377.2	58.9	0.8
12	0	0	0	0	0	0	0	0	0	0	0	-30	0	0	0	0	0	0	0	0	0	-378.1	158.2	-384.6	52.6	0.7
13	0	0	0	0	0	0	-10	0	0	0	0	-30	30	0	0	0	0	0	0	0	30	-376.3	160.1	-381.7	42.8	1.2
14	0	0	0	0	0	0	0	0	0	0	-90	-30	30	0	0	0	0	0	0	0	0	-383.5	147.4	-372.8	50.9	0.9
15	10	0	0	0	0	0	0	0	0	0	0	0	-30	30	0	0	0	0	0	0	0	-370.5	131.3	-374.6	40.7	1.1
16	0	0	0	10	0	0	0	0	0	0	0	-30	0	0	0	0	0	30	0	0	0	-381.1	143.5	-369.2	43.5	1.1
17	10	0	0	-10	0	0	0	0	0	0	-90	-30	30	0	0	0	0	0	0	0	30	-380.7	165.4	-376.1	51.4	1.3
18	10	0	0	0	0	0	0	0	0	0	30	0	-30	30	0	0	0	0	0	0	0	-367.3	135.6	-371.5	42.9	1.1
19	0	0	0	0	0	0	0	0	0	0	30	-30	60	0	0	0	0	0	0	0	0	-381.4	164.3	-382.1	73.7	1.0
20	0	0	0	-10	0	0	0	0	0	0	-30	-30	30	0	0	0	0	0	0	0	0	-387.8	170.2	-379.0	73.0	1.0
21	0	0	0	0	10	0	0	0	0	0	-60	0	0	0	0	0	0	0	0	0	0	-381.7	178.8	-384.5	67.7	0.8
22	0	0	0	0	0	0	0	0	0	0	0	0	-30	0	0	0	0	0	0	0	0	-365.8	149.0	-370.3	40.2	0.5
23	-10	0	0	0	0	0	-10	0	0	0	30	-30	60	0	-30	0	0	0	0	0	30	-383.3	178.1	-382.1	75.6	1.5
24	10	0	0	0	0	0	-10	0	0	0	0	-30	30	0	0	0	0	0	0	0	0	-364.5	140.7	-367.4	40.3	1.3
25	0	0	0	0	0	0	0	0	0	0	0	0	0	0	0	0	0	0	0	0	0	-375.8	178.0	-374.6	70.4	0.0

Table S5. Top 25 structures for TAS1R2 taste receptor from SuperBihelix ranked by the average rank of the charged total (CTot), neutralized total (Ntot), charged interhelical (CIH), and neutralized interhelical (NIH) energy. Theta, θ, (tilt), phi, ϕ, (sweep), eta, η, (rotation) angles and the backbone RMSD (Å) with respect to the starting conformation. All structures are from mGluR5-top1 in BiHelix run.

#	θ (tilt)							ϕ (sweep)							η (rotation)							CIH	CTot	NIH	NTot	RMSD
	H1	H2	H3	H4	H5	H6	H7	H1	H2	H3	H4	H5	H6	H7	H1	H2	H3	H4	H5	H6	H7					
1	0	0	0	-10	0	0	0	0	0	0	-60	0	0	0	0	0	0	0	0	0	0	-460.1	144.5	-407.8	121.6	0.7
2	0	0	0	-10	0	0	0	0	0	0	-30	0	0	0	0	0	0	-30	0	0	0	-445.4	141.6	-406.9	107.4	0.9
3	0	0	0	0	0	0	0	0	0	0	30	0	0	0	0	0	0	-30	0	0	0	-438.5	107.7	-402.3	75.9	0.5
4	10	0	0	-10	0	0	0	0	0	0	-30	0	0	0	-30	0	0	-30	0	0	0	-452.9	166.3	-406.7	130.9	1.2
5	0	0	0	0	0	0	0	0	0	0	0	0	0	0	30	0	0	-30	0	0	0	-435.9	144.9	-395.6	119.0	0.7
6	0	0	0	-10	0	0	0	0	0	0	-60	-30	0	0	0	0	0	-30	0	0	0	-468.1	177.6	-410.9	135.3	1.0
7	0	0	0	0	0	0	0	0	0	0	30	0	0	0	0	0	0	0	0	0	0	-443.7	167.1	-396.9	153.4	0.3
8	0	0	0	0	0	0	0	0	0	0	90	0	0	0	0	0	0	0	0	0	0	-442.0	172.3	-394.3	148.2	0.6
9	0	0	0	-10	10	0	0	0	0	0	-30	0	0	0	0	0	0	-30	-30	0	0	-437.8	171.8	-388.6	135.1	1.2
10	0	0	0	-10	0	0	0	0	0	0	-30	0	0	0	0	0	0	0	0	0	0	-447.6	177.1	-403.7	157.0	0.7
11	10	0	0	0	0	0	0	0	0	0	0	0	0	0	0	0	0	0	0	0	0	-432.5	153.5	-386.7	134.7	0.8
12	0	0	0	-10	0	0	0	0	0	0	-60	0	0	0	30	0	0	0	0	0	0	-442.1	165.0	-388.6	165.9	0.8
13	0	0	0	0	0	0	0	0	0	0	0	-30	0	0	0	0	0	-30	0	0	0	-428.6	157.3	-387.2	120.5	0.8
14	10	0	0	-10	0	0	0	0	0	0	-60	0	0	0	0	0	0	0	0	0	0	-445.8	176.4	-383.6	158.2	1.0
15	0	0	0	-10	10	0	0	0	0	0	-60	0	0	0	0	0	0	0	-30	0	0	-450.8	171.9	-385.9	166.9	1.0
16	0	0	0	0	0	0	0	0	0	0	60	0	0	0	0	0	0	0	0	0	0	-437.1	151.0	-376.0	148.7	0.5
17	10	0	0	-10	0	0	0	0	0	0	-60	0	0	0	-30	0	0	0	0	0	0	-446.7	181.5	-397.1	162.1	1.1
18	0	0	0	0	10	0	0	0	0	0	0	0	0	0	0	0	0	-30	-30	0	0	-432.6	168.1	-383.5	142.7	1.0
19	0	0	0	0	0	0	0	0	0	0	0	-30	-30	0	0	0	0	-30	0	-30	0	-440.2	183.6	-381.0	146.9	1.0
20	0	0	0	-10	0	0	0	0	0	0	-60	-30	0	0	0	0	0	0	0	0	0	-449.2	191.2	-402.2	159.2	0.9
21	0	0	0	0	0	0	0	0	0	0	60	0	0	0	0	0	0	-30	0	0	0	-428.4	157.1	-379.0	135.8	0.6
22	0	0	0	0	0	0	0	0	0	0	30	0	0	0	-30	0	0	0	0	0	0	-434.3	168.7	-379.7	158.6	0.5
23	0	0	0	-10	0	0	0	0	0	0	-90	0	0	0	0	0	0	0	0	0	0	-432.2	177.0	-383.1	148.3	0.6
24	0	0	0	-10	0	0	0	0	0	0	30	0	0	0	0	0	0	-30	0	0	0	-436.7	190.5	-400.0	149.9	0.9
25	10	0	0	0	0	0	0	0	0	0	60	0	0	0	-30	0	0	-30	0	0	0	-427.0	171.9	-387.2	146.6	1.0

Table S6. Top 25 structures for TAS1R3 taste receptor from SuperBihelix ranked by the average rank of the charged total (CTot), neutralized total (Ntot), charged interhelical (CIH), and neutralized interhelical (NIH) energy. Theta, θ, (tilt), phi, ϕ, (sweep), eta, η, (rotation) angles and the backbone RMSD (Å) with respect to the starting conformation. All structures are from mGluR1-top1 except Top 22 from mGluR1-top12 in BiHelix run.

#	θ (tilt)							ϕ (sweep)							η (rotation)							CIH	CTot	NIH	NTot	RMSD
	H1	H2	H3	H4	H5	H6	H7	H1	H2	H3	H4	H5	H6	H7	H1	H2	H3	H4	H5	H6	H7					
1	0	0	0	0	0	0	0	0	0	0	90	0	-30	0	0	0	0	0	0	30	0	-584.0	-49.7	-410.3	-57.1	0.8
2	0	0	0	0	0	0	0	0	0	0	90	0	-30	0	0	0	0	0	0	0	0	-558.0	-72.7	-396.0	-88.8	0.7
3	0	0	0	0	0	0	0	0	0	0	0	0	0	0	0	0	0	0	0	0	0	-572.0	-57.4	-392.8	-54.1	0.0
4	0	0	0	0	0	0	0	0	0	0	0	0	-60	0	0	0	0	0	0	30	0	-585.6	-33.7	-411.3	-35.2	0.9
5	0	0	0	0	0	0	0	0	0	0	0	0	-30	0	0	0	0	0	0	0	0	-568.4	-57.2	-387.3	-56.6	0.5
6	0	0	0	0	0	0	0	0	0	0	0		-30	0	0	0	0	0	0	30	0	-577.2	-23.2	-407.2	-32.3	0.7
7	0	0	0	0	0	0	0	0	0	0	60	0	-60	0	0	0	0	0	0	30	0	-583.4	-23.4	-399.7	-24.6	1.0
8	0	0	0	0	0	0	0	0	0	0	90	0	-60	0	0	0	0	0	0	30	0	-574.6	-14.1	-406.7	-27.1	1.0
9	0	0	0	10	0	0	0	0	0	0	0	0	-60	0	0	0	0	0	0	0	0	-546.7	-28.7	-386.8	-42.4	1.1
10	0	0	0	0	0	0	0	0	0	0	90	0	-60	0	0	0	0	0	0	0	0	-556.2	-5.6	-388.3	-21.5	0.9
11	0	0	0	0	0	0	0	0	0	0	0	0	-60	0	0	0	0	0	0	0	0	-553.1	-5.2	-387.8	-21.7	0.8
12	0	0	0	0	0	0	0	0	0	0	60	0	-60	0	0	0	0	0	0	0	0	-562.6	-14.6	-380.2	-17.2	0.9
13	0	0	0	-10	0	0	0	0	0	0	-90	0	-30	0	0	0	0	0	0	0	0	-535.6	-13.3	-375.1	-50.2	0.7
14	0	0	0	0	0	0	0	0	0	0	0	0	-60	0	30	0	0	0	0	0	0	-547.7	12.1	-382.3	2.1	0.9
15	10	0	0	0	0	0	0	0	0	0	90	0	-60	0	-30	0	0	0	0	0	0	-545.8	15.0	-381.4	-4.6	1.3
16	10	0	0	0	0	0	0	0	0	0	90	0	-60	0	0	0	0	0	0	0	0	-545.4	21.2	-386.1	-2.9	1.2
17	0	0	0	0	0	0	0	0	0	0	30	0	-60	0	0	0	0	0	0	0	0	-549.0	11.6	-373.8	-0.1	0.8
18	0	0	0	-10	0	0	0	0	0	0	-90	0	-60	0	0	0	0	0	0	0	0	-533.3	-5.3	-376.5	-35.7	0.9
19	0	0	0	0	0	0	0	0	0	0	90	0	-30	30	0	0	0	0	0	30	0	-544.7	15.4	-369.8	9.2	1.1
20	0	0	0	-10	0	0	0	0	0	0	-90	0	-30	0	0	0	0	0	0	30	0	-539.4	13.1	-367.8	-3.7	0.8
21	0	0	0	0	0	0	0	0	0	0	60	0	-90	0	0	0	0	0	0	0	0	-542.7	10.3	-357.7	13.1	1.1
22	0	0	0	0	0	0	0	0	0	0	0	0	0	0	0	0	0	0	0	0	0	-509.9	-36.8	-391.2	-75.7	0.0
23	0	0	0	-10	0	0	0	0	0	0	-90	0	-60	0	0	0	0	0	0	30	0	-532.1	30.1	-378.2	-12.3	1.0
24	10	0	0	0	0	0	0	0	0	0	0	0	-60	0	-30	0	0	0	0	0	0	-535.3	24.2	-365.1	12.1	1.2
25	0	0	0	0	0	0	0	0	0	0	0	0	-90	0	0	0	0	0	0	0	0	-541.4	25.9	-361.7	31.1	1.1

Table S7. The interhelical polar interactions for the top 25 TMD conformations for TAS1R1 from the SuperBiHelix analysis. The tilt (θ, φ) and rotation (η) angles for these 25 are given in Table S4. We see that all cases have a strong R3.46 to E6.33 salt bridge, except #22 where it is clearly broken, and for #10, #7, and perhaps #13 where it is long. Thus these 1 to 4 structures (shown in grey) might be candidates for active conformation are. The H-bond distances (Å) between pairs of hetero atoms were measured.

#	T3.37-N5.47	Q4.53-N5.47	T1.44-S2.56	R2.41-Q3.49	C2.43-Y7.49	N6.44-S7.48	E6.33-K7.53	E6.33-Y7.49	R3.46-E6.33
1*	3.5	2.9	3.0	2.7	3.8	2.8	15.7	11.5	**2.8**
2	3.5	3.4	2.9	2.7	12.0	4.3	11.0	5.4	**2.6**
3	3.0	2.9	16.0	9.0	4.7	2.8	2.9	2.7	**2.8**
4	3.2	5.1	16.0	8.1	6.9	6.8	2.8	2.9	**2.6**
5	2.9	2.8	16.0	8.6	5.5	6.0	2.8	2.8	**2.7**
6	3.2	5.6	16.0	2.9	4.1	6.8	2.7	2.7	**2.7**
7*	3.7	3.2	16.1	4.8	4.8	5.0	2.8	4.4	**3.2**
8*	3.5	2.8	12.6	10.2	3.6	5.0	2.7	3.6	**2.8**
9	3.7	3.2	16.0	8.1	5.7	6.8	2.7	2.7	**2.6**
10	3.7	3.2	3.0	7.8	3.7	2.9	13.9	10.3	**3.4**
11	3.2	5.4	16.0	5.1	5.0	6.8	2.7	2.8	**2.7**
12	3.5	3.3	16.0	9.1	5.7	6.0	5.2	3.7	**2.7**
13	3.2	5.2	3.0	3.2	4.8	3.7	8.3	11.1	**3.0**
14	3.2	4.3	16.0	7.8	4.1	6.8	2.7	2.7	**2.7**
15	3.5	3.0	16.1	9.4	3.0	6.2	7.8	6.4	**2.6**
16	2.8	4.6	16.0	9.1	4.6	6.0	3.0	4.8	**2.8**
17	3.7	3.0	16.1	7.3	6.7	4.3	13.6	8.2	**2.8**
18	3.5	2.9	16.1	10.4	3.0	6.2	7.8	6.4	**2.6**
19	3.7	3.2	16.0	3.1	6.0	6.0	6.2	2.8	**2.7**
20	3.2	2.9	16.0	3.1	6.3	6.8	8.6	4.6	**2.7**
21	4.6	2.7	16.6	9.5	3.5	2.8	6.6	2.8	**2.7**
22	3.0	2.9	16.0	9.5	4.1	4.5	2.9	5.0	**6.8**
23	3.7	3.2	5.5	7.4	5.1	4.0	15.3	12.9	**2.6**
24	3.5	3.4	14.5	5.1	4.7	5.0	5.0	3.4	**2.7**
25	3.5	2.8	12.5	9.2	3.5	5.5	2.7	3.2	**2.8**

Table S8. The interhelical polar interactions for the top 25 TMD conformations for TAS1R2 from the SuperBiHelix analysis. The tilt (θ, φ) and rotation (η) angles for these 25 are given in Table S5. We see that all cases have a strong R3.46 to E6.33 salt bridge, except #19 and 25 where it is clearly broken, and for #23 where it is long. Thus these 2 to 3 structures (shown in grey) might be candidates for active conformation.

#	Y2.54-S7.50	Q3.29-S5.39	S3.41-T4.50	T3.37-K4.53	T3.37-D5.47	K4.53-D5.47	S6.47-N7.35	C2.43-Y7.53	R3.46-Y7.53	**R3.46-E6.33**	E6.33-Y7.53	E6.33-K7.57
1*	4.5	2.8	2.7	3.3	2.9	2.6	2.8	3.3	4.4	**2.6**	3.6	7.8
2	4.5	5.8	3.8	3.6	3.7	2.6	2.8	4.0	2.7	**2.6**	3.1	4.4
3	4.5	3.8	3.4	2.5	3.1	2.7	2.8	4.0	2.7	**2.6**	3.1	4.4
4	4.8	5.8	3.8	3.6	3.7	2.6	2.8	4.0	2.7	**2.6**	3.1	3.3
5	2.7	3.8	4.9	2.6	3.1	2.7	2.8	3.3	4.5	**2.7**	3.5	2.7
6	4.5	2.8	3.0	2.6	3.2	2.7	2.8	3.4	2.9	**2.7**	3.8	3.3
7	4.5	3.0	3.8	3.3	3.0	2.7	2.8	3.2	3.1	**3.0**	3.7	3.1
8	4.5	3.9	3.0	3.3	3.0	2.5	2.8	3.0	3.0	**3.0**	3.5	2.8
9*	4.5	4.4	2.8	3.7	4.4	2.6	2.8	3.4	2.9	**2.7**	3.8	3.3
10	4.5	2.7	2.8	5.5	5.1	2.6	2.8	3.3	4.5	**2.8**	3.5	2.9
11	5.3	2.9	3.1	3.4	3.0	2.7	2.8	3.3	4.9	**2.6**	4.1	2.8
12	2.7	2.8	2.7	3.3	2.9	2.7	2.8	3.3	4.5	**2.6**	3.6	2.8
13	4.8	3.0	4.9	2.6	3.0	2.7	2.8	3.8	2.9	**2.7**	3.8	5.1
14	4.4	4.8	2.7	3.3	2.9	2.6	2.8	3.3	4.4	**2.6**	2.8	2.7
15	4.5	5.6	2.7	4.0	4.2	2.7	2.8	3.5	2.9	**2.6**	3.2	3.2
16	4.5	4.4	3.1	3.3	3.0	2.6	2.8	3.9	3.9	**2.7**	2.7	2.8
17	4.8	4.7	2.7	3.3	2.9	2.7	2.8	3.3	3.3	**2.7**	3.5	2.7
18	4.5	3.9	3.4	4.9	4.3	2.7	2.8	4.4	2.7	**2.6**	3.1	3.3
19*	4.5	4.7	3.4	3.0	3.2	2.7	4.7	5.9	4.1	**6.2**	3.0	2.6
20	4.5	3.0	2.7	3.4	3.3	2.7	2.8	3.4	3.1	**2.7**	4.4	5.1
21	4.5	4.9	3.4	2.8	3.2	2.6	2.8	4.7	4.2	**2.9**	2.7	4.4
22	3.1	2.9	3.8	3.3	3.0	2.6	2.8	3.5	3.7	**2.7**	3.1	3.2
23	4.5	3.9	3.0	3.3	3.0	2.5	2.8	4.1	3.5	**4.2**	2.9	3.2
24	4.5	4.3	2.9	4.0	3.1	2.7	2.8	3.9	3.7	**2.7**	3.1	2.8
25	4.8	4.9	3.4	2.5	3.1	2.7	2.8	3.3	3.6	**9.1**	6.9	2.8

Table S9. The interhelical polar interactions for the top 25 TMD Bundles for TAS1R3 from the SuperBiHelix analysis. The tilt (θ, φ) and rotation (η) angles for these 25 are given in Table S6. Here the R3.46 and E6.33 of 1R1 and 1R2 are replaced with Q3.46 and R6.33. Thus we obtain a HB not a salt bridge. Now all cases except #2, 12, 13, 15, 16, and 17 have clearly broken 3-6 interactions making these 19 structures candidates for active conformation. However, we observe a TM 3-4 salt-bridge between E3.49 and R4.40 in 20 structures except #13, 18, 20, 22 and 23. TAS1R3 has the fewest inter-helical constraints among TAS1Rs. Based on these analyses we might expect #18, 20, 22 and 23 without TM3-4 and TM3-6 interactions (shown in grey) to be the best candidates for active structures.

#	Q3.29-S5.39	E4.55-N5.47	T3.37-N5.47	T3.37-E4.55	**E3.49-R4.40**	E3.53-R4.40	**Q3.46-R6.33**
1*	3.4	5.6	3.2	5.4	**2.7**	2.7	**7.4**
2	4.4	6.7	3.0	3.5	**2.7**	2.7	**4.0**
3	3.4	6.4	3.2	2.7	**3.0**	2.6	**6.9**
4	3.4	5.1	2.8	3.4	**3.0**	2.6	**9.6**
5	4.1	3.6	3.0	3.0	**3.0**	2.6	**8.8**
6	4.1	3.6	3.2	3.4	**3.0**	2.6	**12.3**
7	3.4	5.5	3.2	5.5	**3.0**	2.6	**9.1**
8	4.6	3.4	3.2	3.2	**2.7**	2.7	**9.8**
9	2.8	3.0	2.8	2.7	**3.0**	5.9	**6.9**
10	4.6	4.9	2.6	3.4	**2.7**	2.7	**7.5**
11	3.4	3.7	3.0	3.4	**3.0**	2.6	**6.2**
12	2.8	3.5	2.9	3.2	**3.0**	2.6	**3.7**
13	5.0	6.7	3.0	3.5	**4.9**	2.6	**3.0**
14	3.4	3.7	3.0	3.4	**3.0**	2.6	**8.6**
15*	4.6	3.4	3.2	3.2	**2.7**	2.7	**3.3**
16	4.6	3.4	3.2	3.2	**2.7**	2.7	**3.3**
17	2.8	3.3	2.5	2.6	**2.9**	3.1	**3.7**
18	4.6	5.4	3.0	3.5	**4.9**	2.6	**7.5**
19	5.0	4.8	3.2	4.9	**2.7**	2.7	**6.5**
20	5.0	3.3	3.3	3.0	**4.9**	2.6	**10.5**
21	4.6	5.6	3.2	5.4	**3.0**	2.6	**10.4**
22*	2.8	14.8	2.8	12.7	**12.1**	21.2	**11.0**
23	5.0	5.5	3.0	3.5	**4.9**	2.6	**9.2**

24	3.4	3.7	2.9	3.6	**3.0**	2.6	**5.5**
25	3.4	3.7	3.2	3.6	**3.0**	2.6	12.2

Table S10. Allosteric ligands to bind to transmembrane domains (TMD) of type 1 taste receptors (TAS1Rs)

#	Compound	Structure	Potencies	Comments	References
1	S807	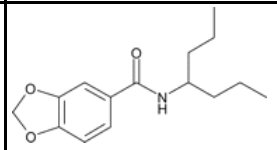	$EC_{50} \approx 0.5$ μM	Allosteric agonist binding to the 7 TMD of TAS1R1 (umami)	(2)
2	S819	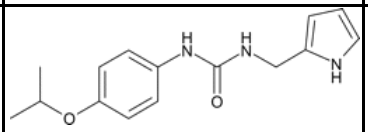	$EC_{50} \approx 25$ μM	Allosteric agonist binding to the 7 TMD of TAS1R2 (sweet)	(2)
3	Lactisole	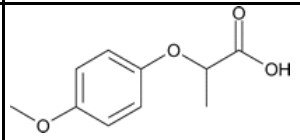	$IC_{50} = 41$ μM	Negative modulator binding to the 7 TMD of TAS1R3 (sweet/umami)	(3, 4)

Table S11. The Top 25 cavity residues of binding for sucrose, stevioside, and Mogroside V. The non-bonding energy (kcal/ mol) in the binding site was calculated. Experiments mutating of D142 and E302 to alanine abolished the activities of sucrose. The common residues which are known are critical residues for sucrose and stevioside activation in the experiment (S40, K65, Y103, D142, D278, E302, P277, and R383 residues) (26) (4) (27) (25) are shown in bold face.

Sucrose						**Stevioside**						**Mogroside V**					
Res.	**#**	**VdW**	**Coulomb**	**H-Bond**	**NonBond**	**Res.**	**#**	**VdW**	**Coulomb**	**H-Bond**	**NonBond**	**Res.**	**#**	**VdW**	**Coulomb**	**H-Bond**	**NonBond**
ASP	**142**	6.79	-3.31	-12.98	-9.51	**ARG**	**383**	4.21	-6.77	-7.93	-10.50	**LYS**	**65**	-2.78	-4.70	-4.08	-11.56
GLU	**302**	7.21	-7.33	-9.27	-9.39	**ASP**	**142**	15.64	-11.03	-14.17	-9.56	GLU	382	3.00	-2.67	-8.36	-8.02
ARG	**383**	4.18	-6.30	-5.63	-7.76	**GLU**	**302**	0.91	-4.84	-4.53	-8.46	GLU	63	-2.91	-3.21	0.00	-6.13
SER	144	4.62	-2.14	-8.03	-5.56	SER	144	-0.70	-1.79	-2.56	-5.05	ASP	307	0.54	-1.86	-4.35	-5.68
TYR	215	-3.09	-0.28	0.00	-3.37	**LYS**	**65**	1.43	-1.47	-4.19	-4.23	**PRO**	**277**	-4.74	-0.65	0.00	-5.39
ASN	143	-2.41	-0.43	0.00	-2.85	LEU	279	-3.02	0.02	0.00	-3.00	ASN	44	3.42	-2.34	-6.38	-5.31
ILE	167	-2.06	-0.07	0.00	-2.13	**SER**	**40**	11.46	-1.98	-12.40	-2.92	**TYR**	**103**	-5.49	0.23	0.00	-5.26
TYR	**103**	-1.58	-0.13	0.00	-1.71	**ASP**	**278**	-2.86	-0.05	0.00	-2.92	**GLU**	**302**	6.37	-2.31	-9.29	-5.23
LYS	**65**	-0.05	-1.56	0.00	-1.61	SER	303	-1.82	-0.77	0.00	-2.58	**ASP**	**142**	-0.20	-0.48	-4.08	-4.76
SER	165	-0.48	-0.53	-0.55	-1.56	TYR	164	-2.26	0.04	0.00	-2.22	LEU	71	-4.04	-0.01	0.00	-4.05
PRO	**277**	-1.47	-0.08	0.00	-1.55	LEU	41	-1.99	0.10	0.00	-1.90	ILE	167	-3.42	-0.53	0.00	-3.95
SER	303	6.86	-3.64	-4.74	-1.51	ASN	44	-1.70	-0.07	0.00	-1.77	VAL	384	-0.72	-0.61	-2.51	-3.84
VAL	384	-1.32	-0.10	0.00	-1.42	LEU	71	-1.49	-0.22	0.00	-1.71	ASN	70	-2.84	-0.98	0.00	-3.82
ILE	67	-1.16	-0.24	0.00	-1.40	ILE	104	-1.51	0.02	0.00	-1.49	**ASP**	**278**	-1.83	-1.49	0.00	-3.32
ASP	218	-0.05	-0.63	0.00	-0.67	ALA	166	-1.27	0.12	0.00	-1.15	TYR	69	-3.07	-0.24	0.00	-3.31
TYR	164	-0.31	-0.11	0.00	-0.42	ASN	143	1.42	-2.27	-0.03	-0.89	TYR	164	-3.04	0.05	0.00	-2.99
ARG	339	0.00	-0.41	0.00	-0.41	THR	242	-0.76	-0.12	0.00	-0.89	LEU	279	-3.09	0.17	0.00	-2.92
ASN	219	-0.22	-0.17	0.00	-0.39	SER	211	-0.83	0.01	0.00	-0.82	SER	165	-3.04	0.39	0.00	-2.64
PRO	141	-0.26	-0.08	0.00	-0.34	ILE	327	-0.83	0.06	0.00	-0.77	ILE	67	-3.05	0.59	0.00	-2.46
VAL	66	-0.13	-0.21	0.00	-0.34	ASN	219	-0.30	-0.38	0.00	-0.68	PHE	373	-2.26	-0.17	0.00	-2.43

Table S12. Five stevioside analogues with experimental results from human sensory studies and from functional taste receptor expression assays sweetness (threshold concentration: µM).(8) Abbrevation: Stev for Stevioside, RebA for Rebauduisude A, Stbs for Steviolbioside, Rubu for Rubusoside, 2H-Stev for 2H-Stevioside

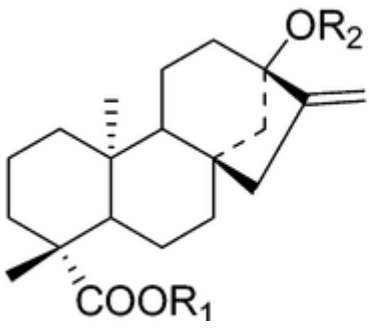

4-7

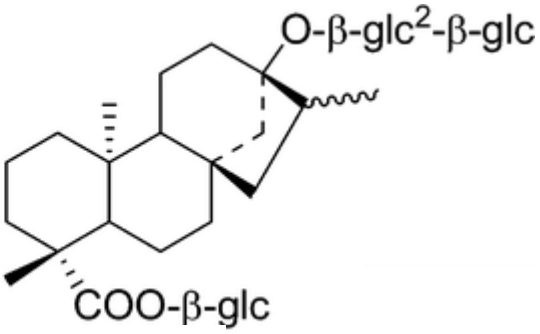

8

#	Compound	R1	R2	human sensory test for sweet	Cell expressing hTAS1R2/hTAS1R3
4	Stev	Gluβ1-	Gluβ1-2Gluβ1-	11.1	4.3
5	RebA	Gluβ1-	Gluβ1-2(Gluβ1-3)Gluβ1-	8.3	4.3
6	Stbs	H	Gluβ1-2Gluβ1-	26.8	12.9
7	Rubu	Gluβ1-	Gluβ1-	27.3	25.9
8	2H-Stev	Gluβ1-	Gluβ1-2Gluβ1-	28.1	38.8

Table S13. The structures of the ligands and the sweetness data for 500 ppm (Grey). All cases started with the same initial conformation of the heterodimer with the 38.7 Å distances for coA. The distances after 10 ns molecular dynamics at 310 K are averaged over the period from 8-10ns. We list the following;

- The average distance (Å) between the geometric center of lower VFD2 and lower VFD3 (Avg lower VFD Dis.) in **Fig. 1**. Here we consider that distances more than 1 Å closer than the 43 Å for the apo case indicate activation. 9 of 10 cases are consistent. The outlier is Rubu.

- The average distance (Å) between the closest Cα of TM6 for TMD2 with a Cα of TM6 for TMD3 (Avg TM6-6' Cα Dis.) in **Fig. 1**. Here we consider that distances more than 2 Å closer than the 9.2 Å for the apo case indicate activation. 8 of 10 cases are consistent. The outliers are Stev, RebM, and RebG (too long).

- The number of Cα of TM6 of TMD2 within 9 Å of the Cα of TM6 of TMD3 (Avg TM6-6' Cα #) from. Here we consider that 4 or shorter contacts indicates activation. 8 of 10 cases are consistent. The outliers are Stev and RebG shown in italics.

- With the shortest TM6–TM6 Cα–Cα distance [decreasing by up to 4.5 Å (MogV) from the 9.2 Å distance in the apo, assuming that a decrease of at least 1 Å indicates activation], we find that 8 of the 10 cases are activated, with the outliers Stev and RebG.
- The number of Cα–Cα distances between the TM6 and two TM6 helices shorter than 9 Å starts out as 0 for the apo protein and ranges up to 18 (MogV). We consider that this must be at least 1 to indicate activation. Eight of the 10 cases satisfy this with outliers Stev and RebG.

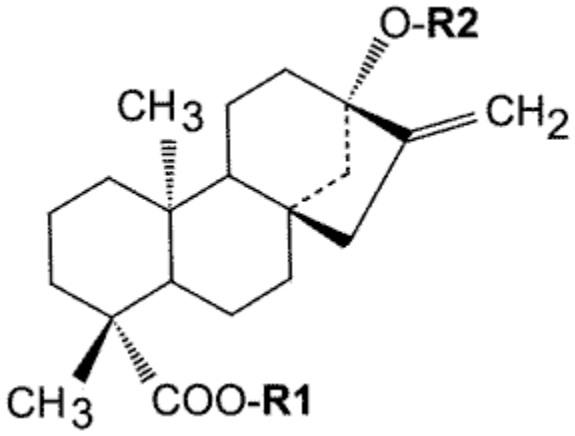

Name	R1 (COO-)	R2 (O-)	Sweetness @ 500 ppm	Avg lower VFD Dis.	Avg TM6-6' Cα Dis.	Avg TM6-6' Cα #
RebM	Gluβ1-2(Gluβ1-3)Gluβ1-	Gluβ1-2(Gluβ1-3)Gluβ1-	**8.19**	40.04	*8.17*	*1.35*
Stev	Gluβ1-	Gluβ1-2Gluβ1-	**7.96**	40.81	*9.86*	*0.00*

RebN	Rhaα1-2(Gluβ1-3)Gluβ1-	Gluβ1-2(Gluβ1-3)Gluβ1-	**7.89**	38.26	6.08	8.60
RebD	Gluβ1-2Gluβ1-	Gluβ1-2(Gluβ1-3)Gluβ1-	**7.66**	37.84	5.79	13.15
MogV*	Gluβ1-2Gluβ1-	Gluβ1-2(Gluβ1-6)Gluβ1-	**7.34**	41.21	4.57	18.40
RebA	Gluβ1-	Gluβ1-2(Gluβ1-3)Gluβ1-	**7.34**	38.64	6.87	5.30
Rubu	Gluβ1-	Gluβ1-	**5.72**	*43.08*	6.56	7.40
RebE	Gluβ1-2Gluβ1-	Gluβ1-2Gluβ1-	**5.6**	41.18	7.58	4.00
RebC	Gluβ1-	Rhaα1-2(Gluβ1-3)Gluβ1-	**3.18**	39.04	5.94	12.00
RebG	Gluβ1-	Gluβ1-3Gluβ1-	**2.51**	37.36	*10.84*	*0.00*
Apo	-	-	**0.00**	43.01	9.23	0.2

- Reb: Rebaudioside, Stev: Stevioside, Rubu: Rubusoside, Mog: Mogroside

* The 2D structure is shown in **Fig. S4**.

* The detailed data for the shortest TM6-TM6 distance and the Cα number of TM6-TM6 distances shorter than 9 Å is shown in **Fig. S11**.

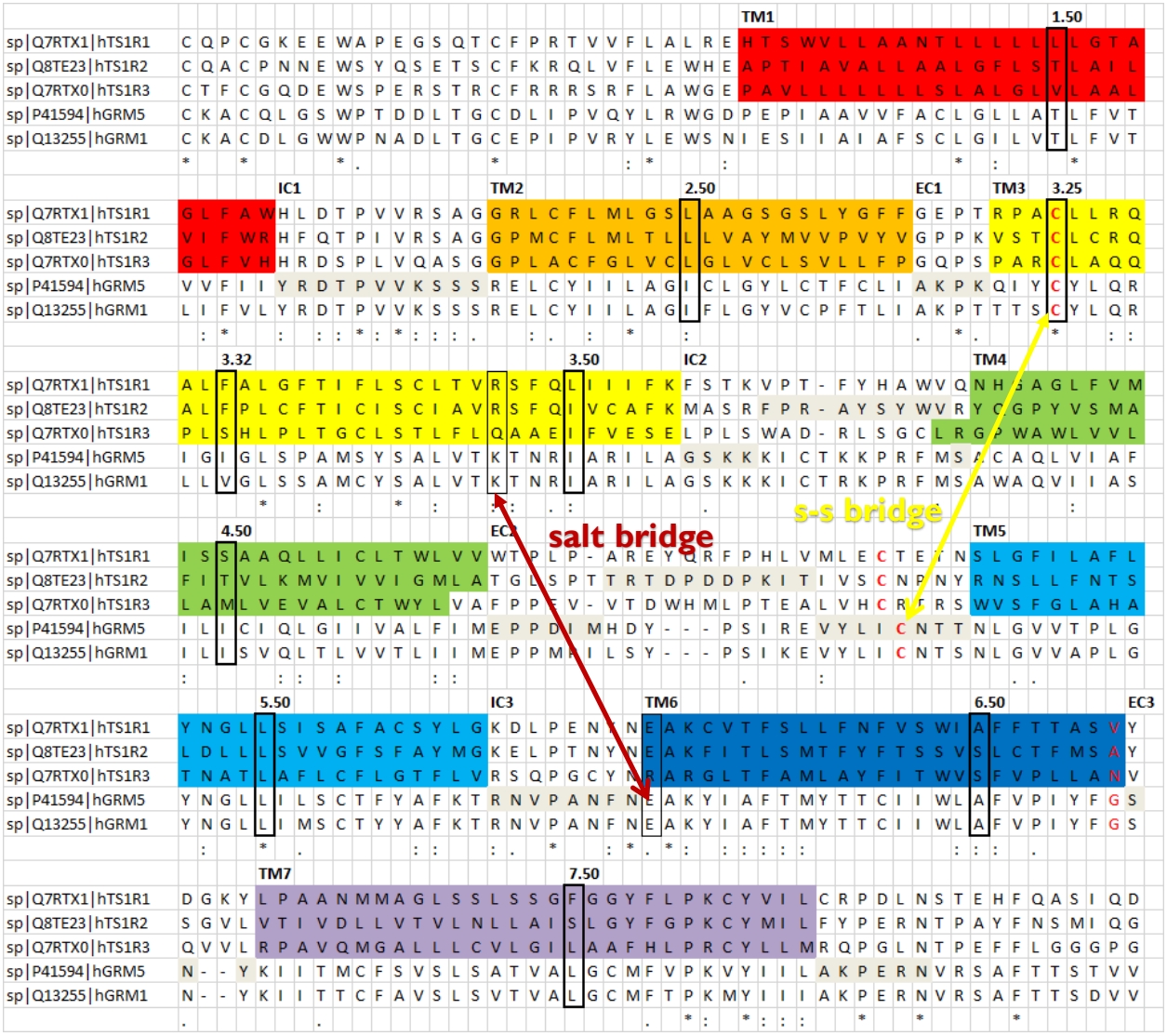

Figure S1. Sequence alignments of the three human TAS1R sweet receptors (hTAS1R1, hTAS1R2, hTAS1R3) with X-ray templates of human metabotropic glutamate receptor (mGluR), mGluR1 and mGluR5 based on the PredicTM method. Most residues of the N- and C-termini are omitted. The predicted transmembrane (TM) regions from PredicTM are displayed in colored boxes. The X.50 residues from Ballesteros-Weinstein numbering (BW#) and the highly conserved residues in all TAS1Rs are shown in black boxes.

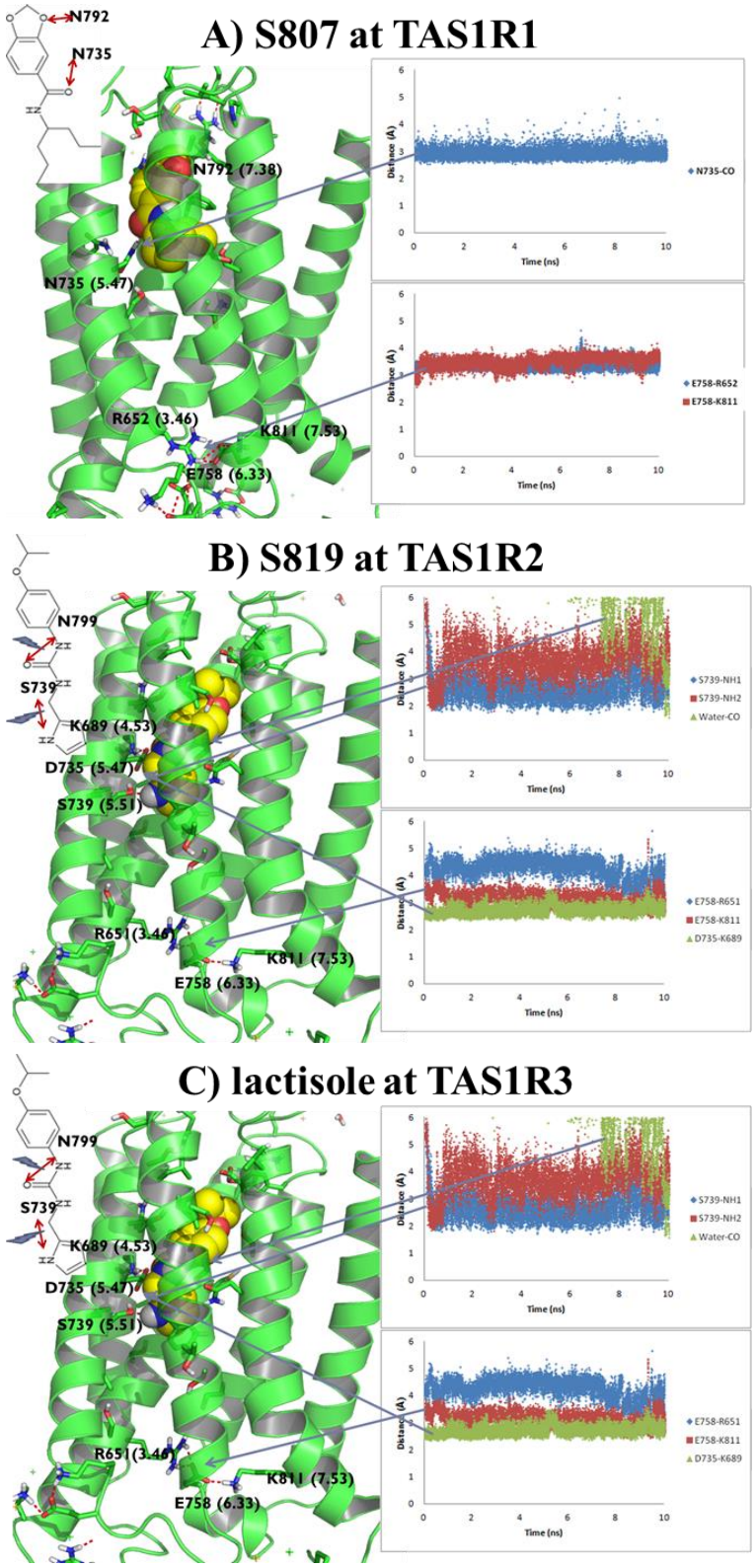

Figure S2. Predicted best binding mode and trajectory analysis of agonist modulators for human taste receptor family (hTAS1R) (A) S807 at hTAS1R1, (B) S819 at hTAS1R2, and (C) lactisole at hTAS1R3.

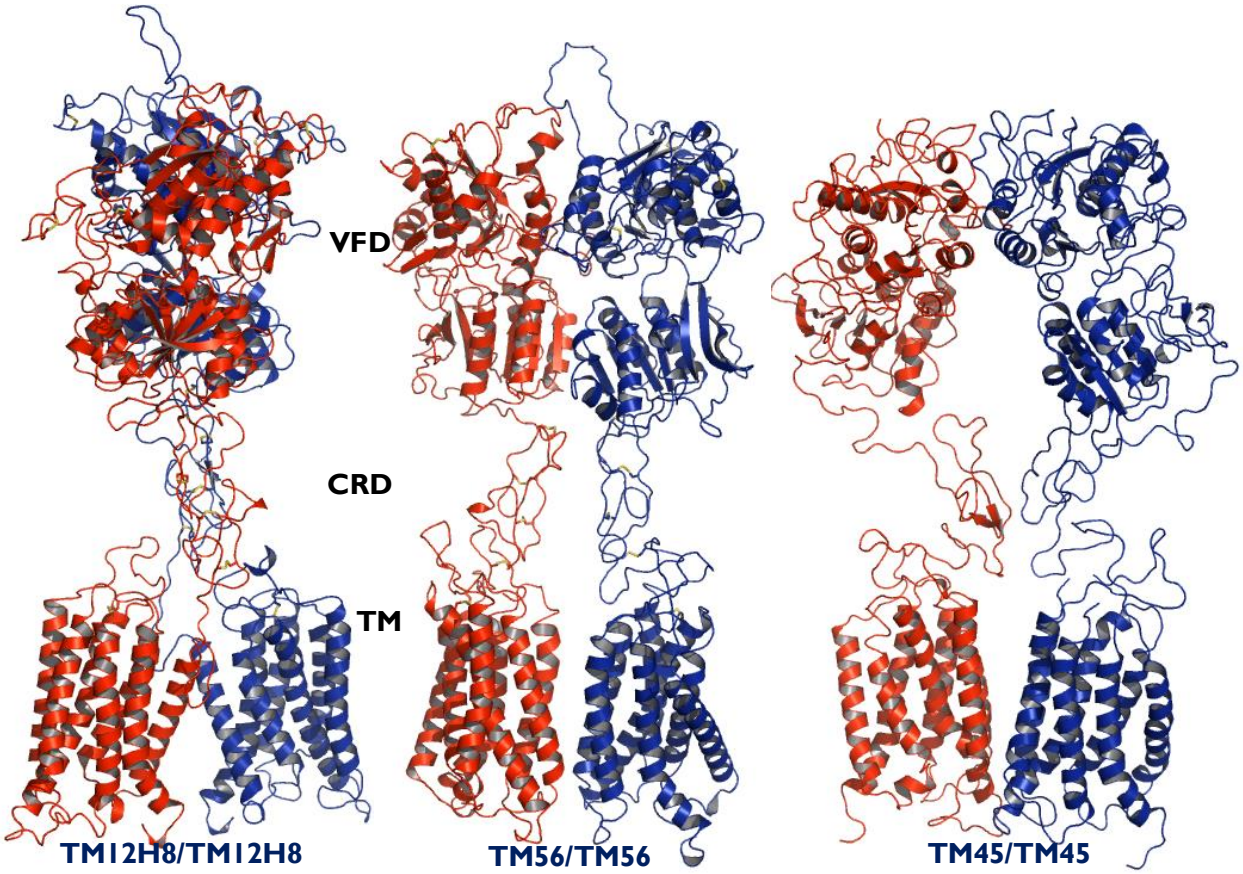

Figure S3. The structure models for the full heterodimers of TAS1R2 (red) and TAS1R3 (blue) including both cysteine-rich domains (CRD) and transmembrane domains (TMD). We consider three interfaces, (a) Model 12co with the "coA" VFD dimer and with interactions between TM1/2 and H8 of each TMD, (b) Model 56co with the "coA" VFD dimer and interactions between TM5/6 of each TMD and (c) Model 45oo with the "ooR" VFD dimer and interactions between TM4/5 of each TMD.

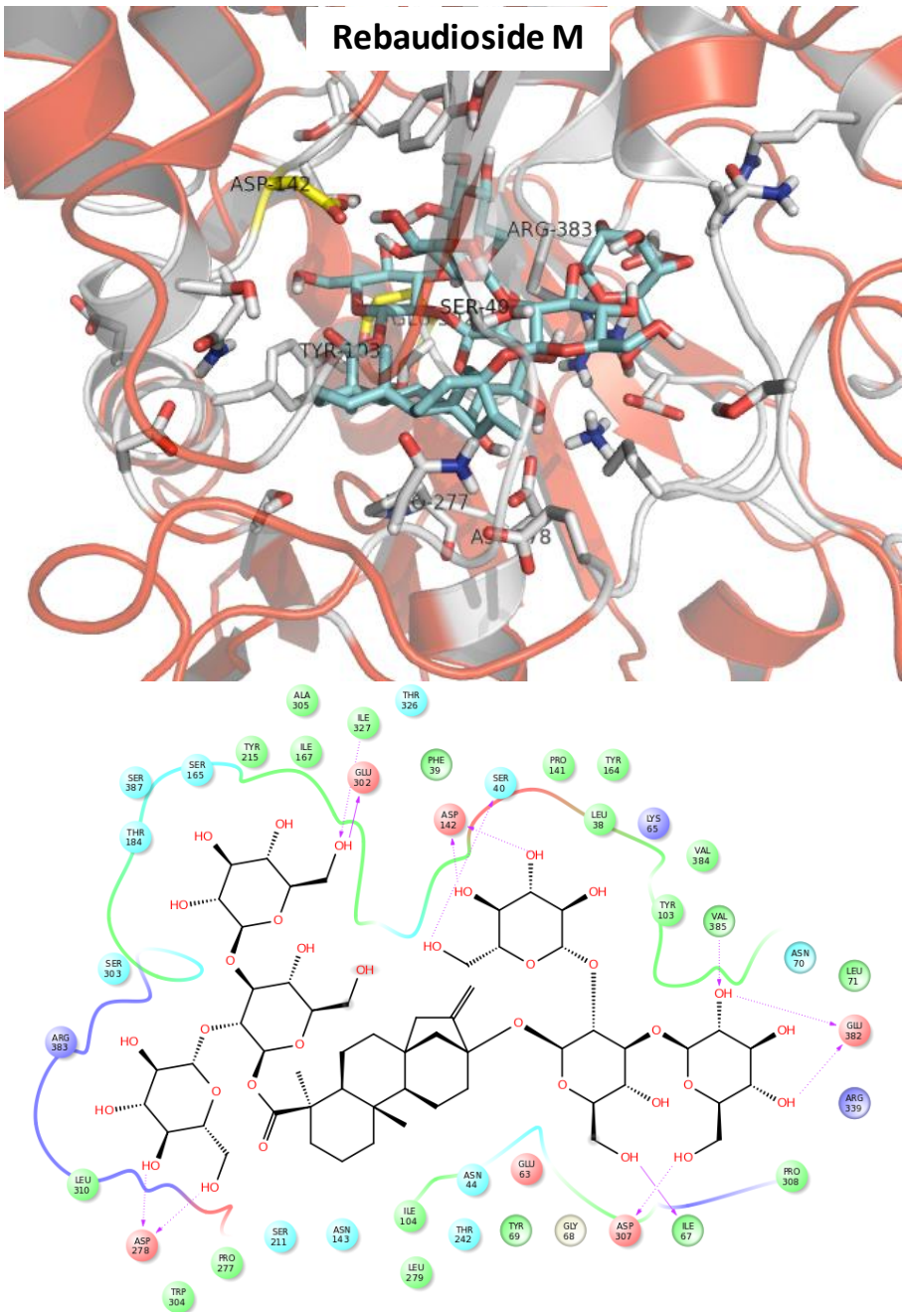
Rebaudioside M
ASP-142
ARG-383
SER-40
TYR-103

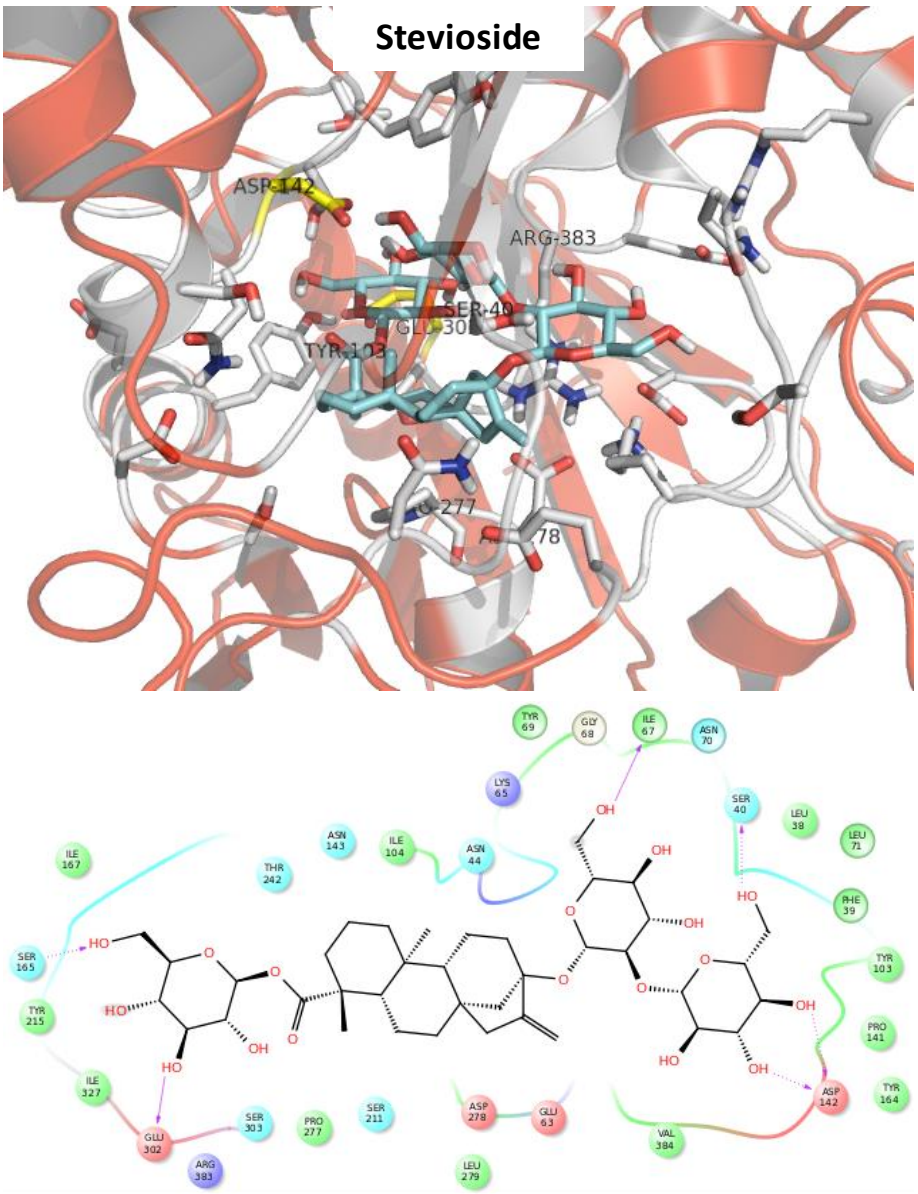
Stevioside
ASP-142
ARG-383
SER-40
GLU-302
TYR-103
TYR 69
GLY 68
ILE 67
ASN 70
LYS 65
SER 40
LEU 38
LEU 71
ASN 143
ILE 104
ASN 44
ILE 167
THR 242
PHE 39
SER 165
TYR 103
TYR 215
PRO 141
ILE 327
SER 303
PRO 277
SER 211
ASP 278
GLU 63
ASP 142
TYR 164
VAL 384
GLU 302
ARG 383
LEU 279

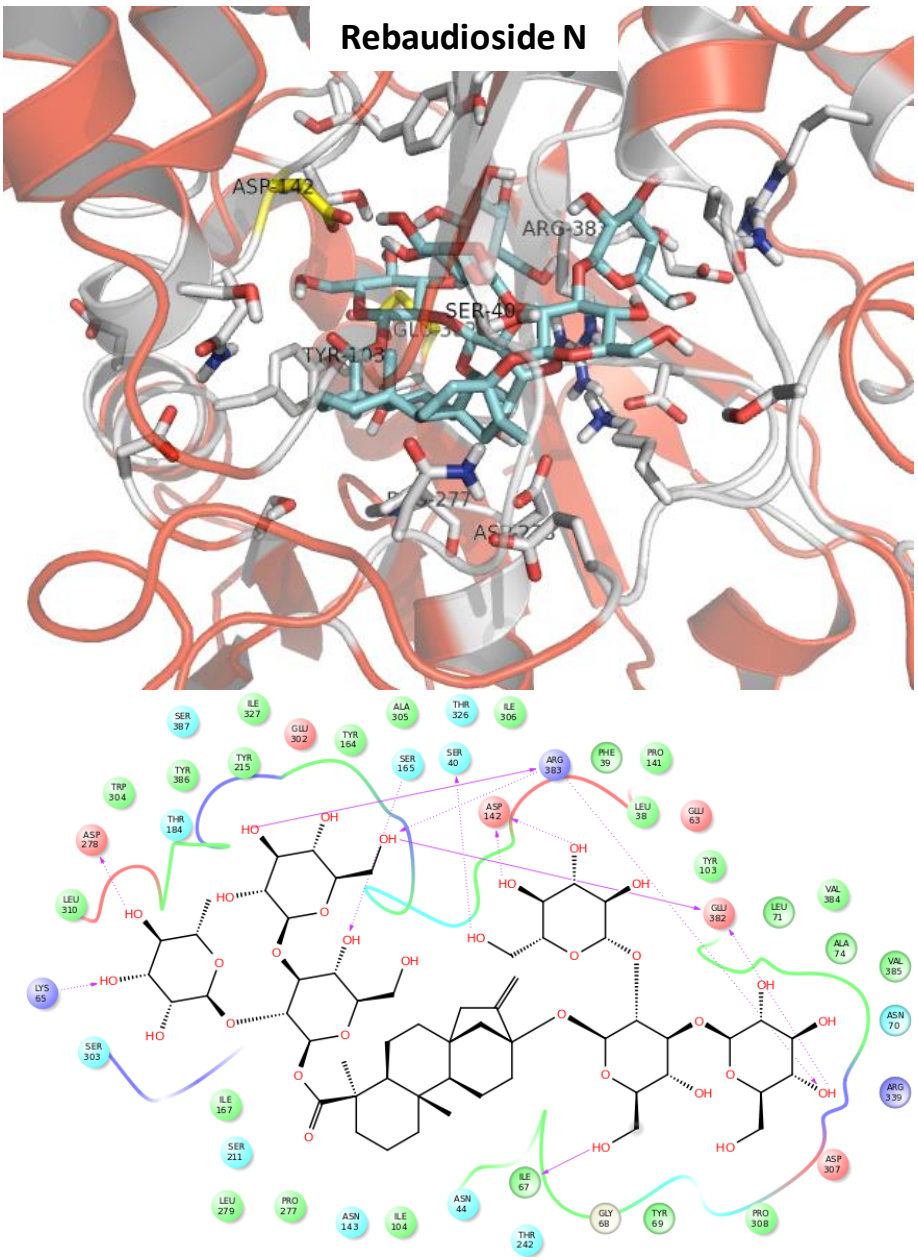
Rebaudioside N
ASP-142
ARG-38
SER-40
TYR-103

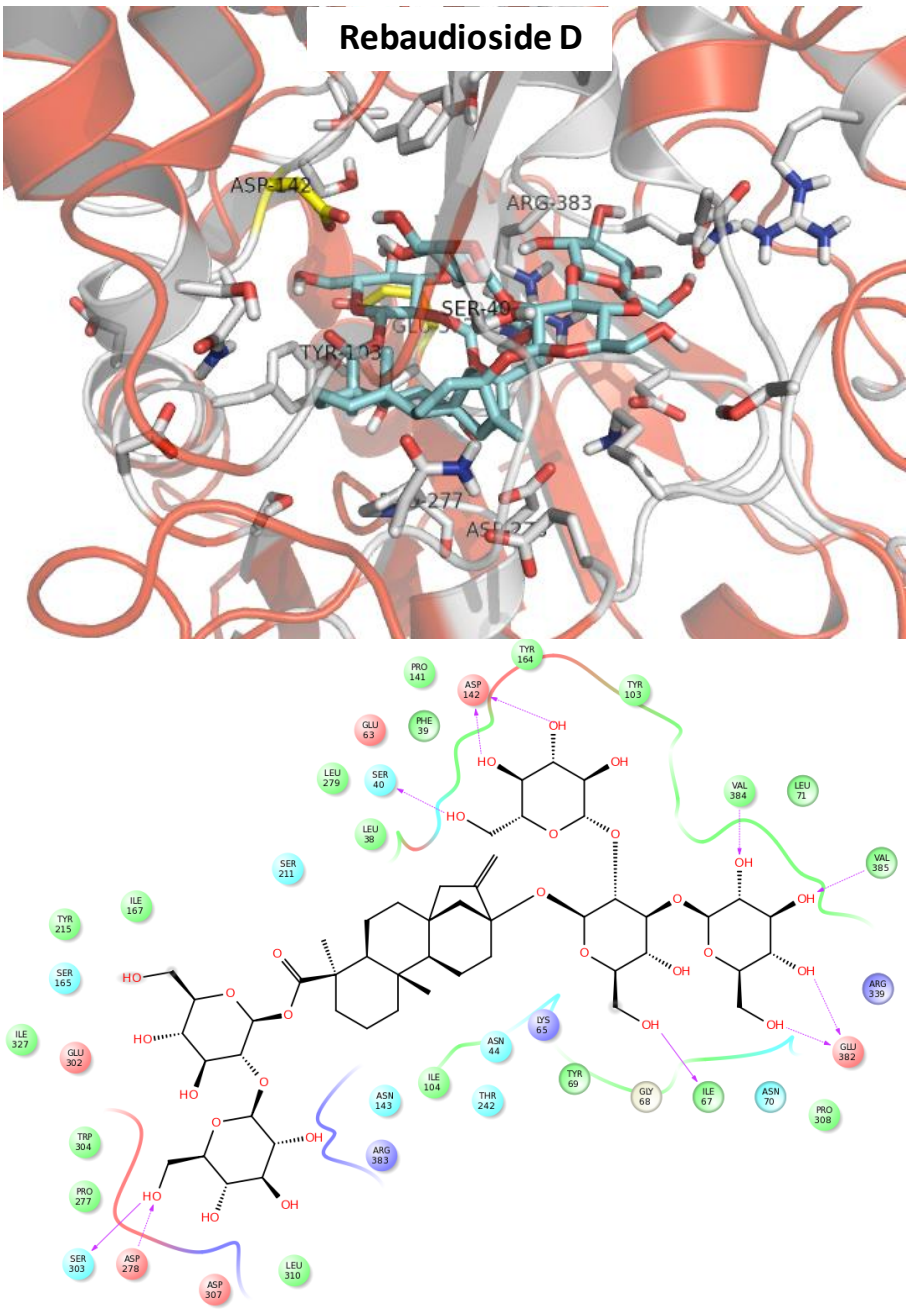
Rebaudioside D
ASP-142
ARG-383
SER-40
TYR-103
-277
TYR 164
PRO 141
ASP 142
TYR 103
GLU 63
PHE 39
LEU 279
SER 40
LEU 38
VAL 384
LEU 71
VAL 385
SER 211
ILE 167
TYR 215
SER 165
ILE 327
GLU 302
ARG 339
LYS 65
ASN 44
ILE 104
TYR 69
GLY 68
ILE 67
ASN 70
PRO 308
GLU 382
THR 242
ASN 143
TRP 304
ARG 383
PRO 277
SER 303
ASP 278
ASP 307
LEU 310

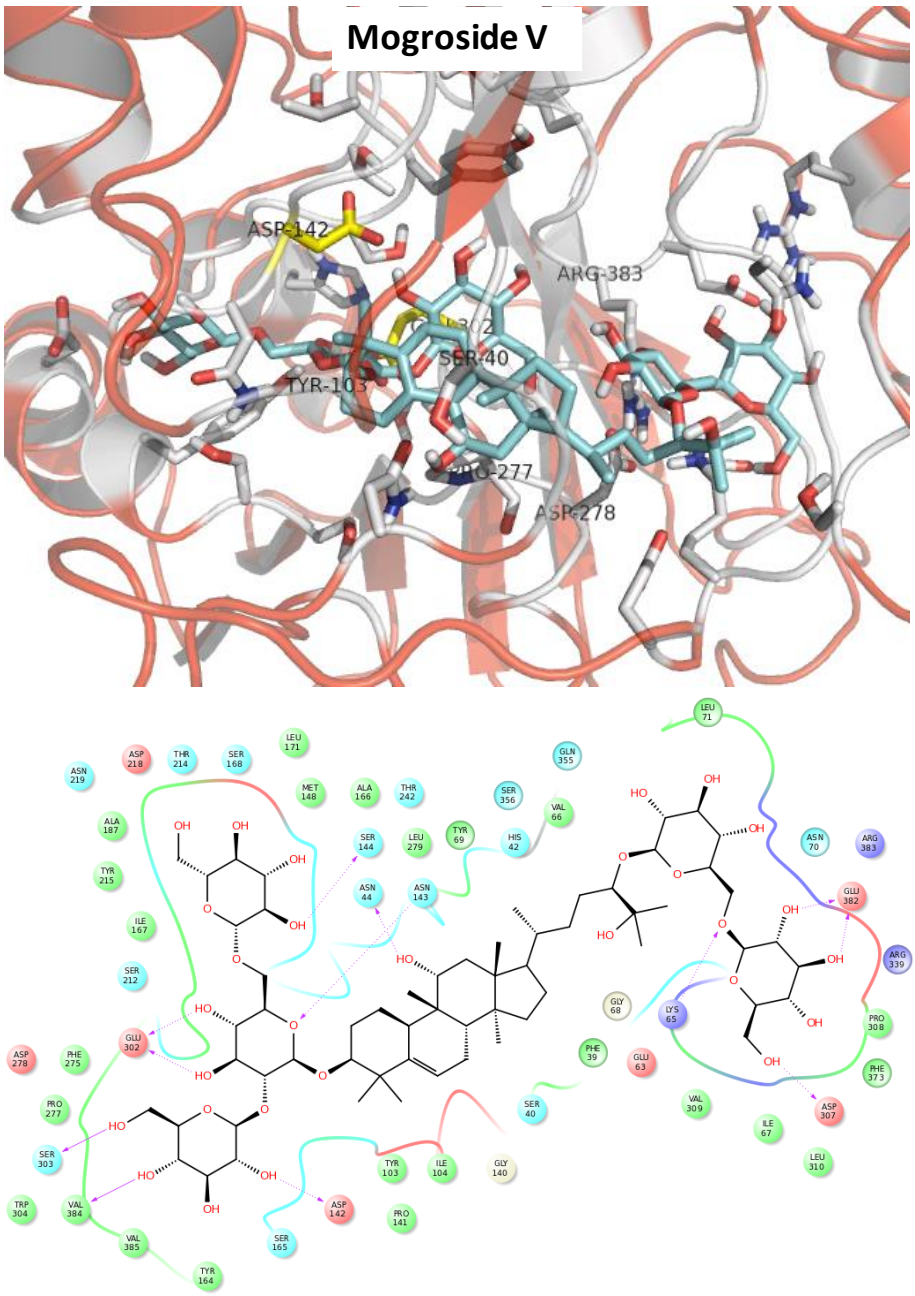
Mogroside V
ASP-142
ARG-383
SER-40
TYR-103
ASP-278

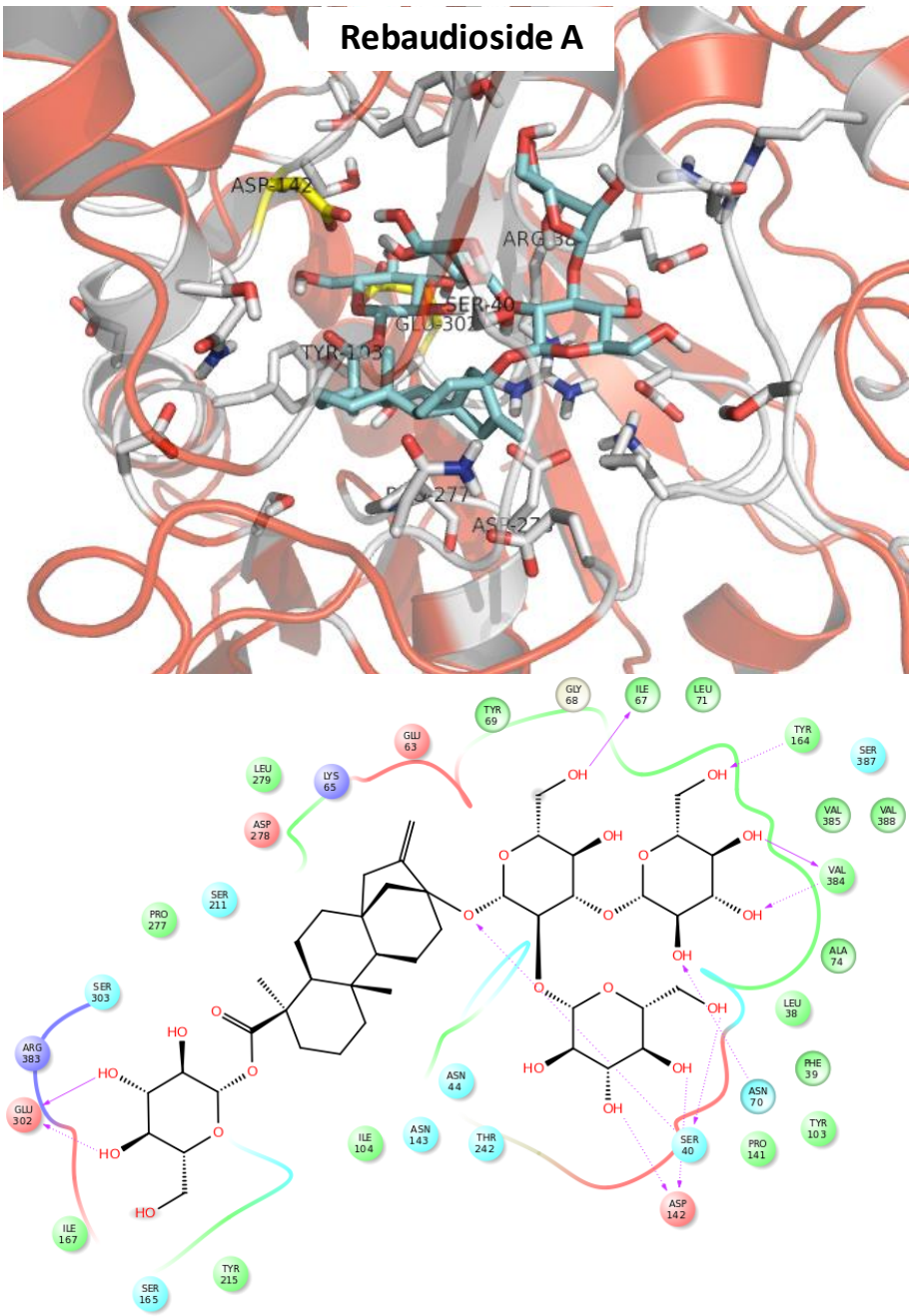
Rebaudioside A
ASP-142
SER-40
TYR-103
GLY
68
ILE
67
LEU
71
TYR
69
GLU
63
TYR
164
SER
387
LEU
279
LYS
65
VAL
385
VAL
388
ASP
278
VAL
384
SER
211
PRO
277
ALA
74
SER
303
LEU
38
ARG
383
PHE
39
ASN
44
ASN
70
GLU
302
TYR
103
ILE
104
ASN
143
THR
242
SER
40
PRO
141
ASP
142
ILE
167
TYR
215
SER
165

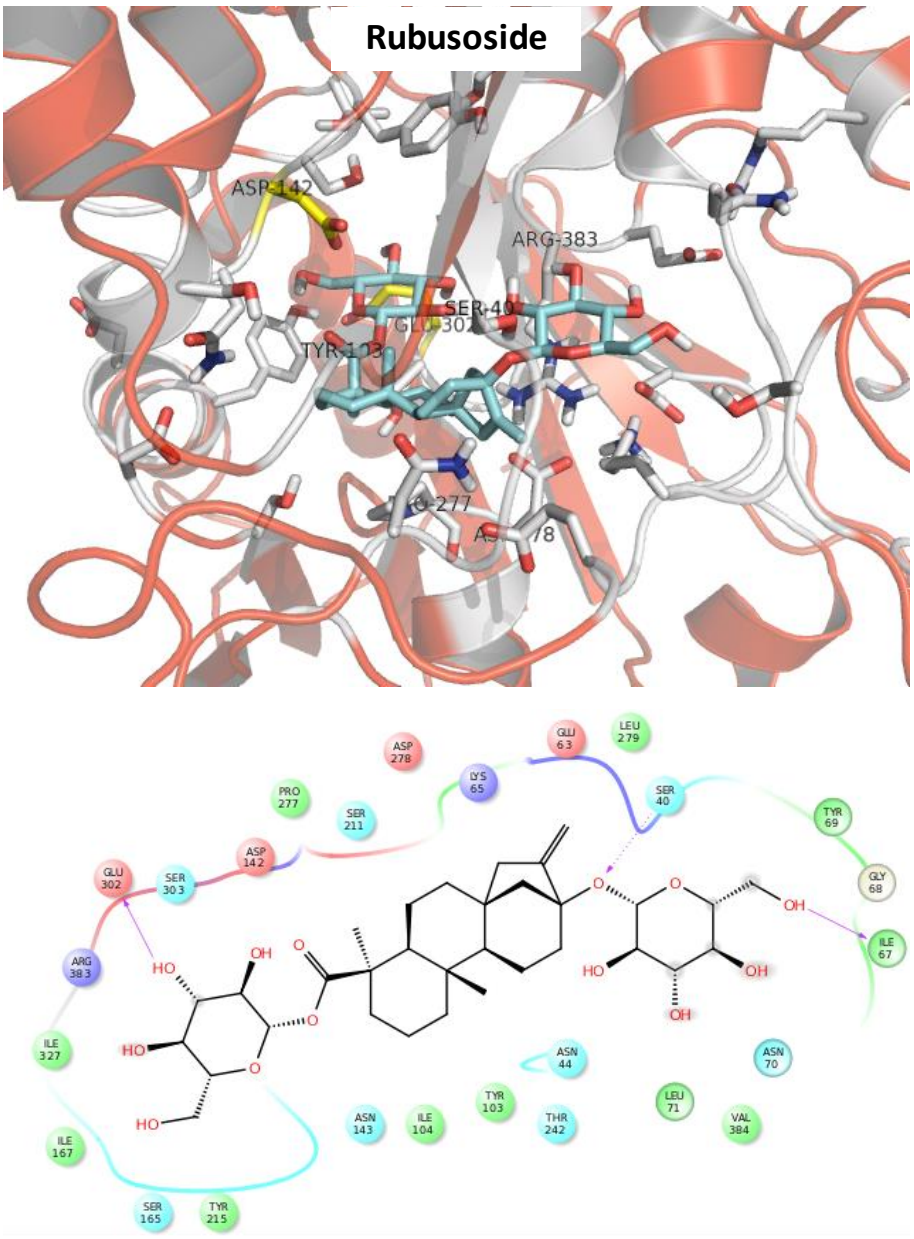
Rubusoside
ASP-142
ARG-383
SER-40
TYR-103

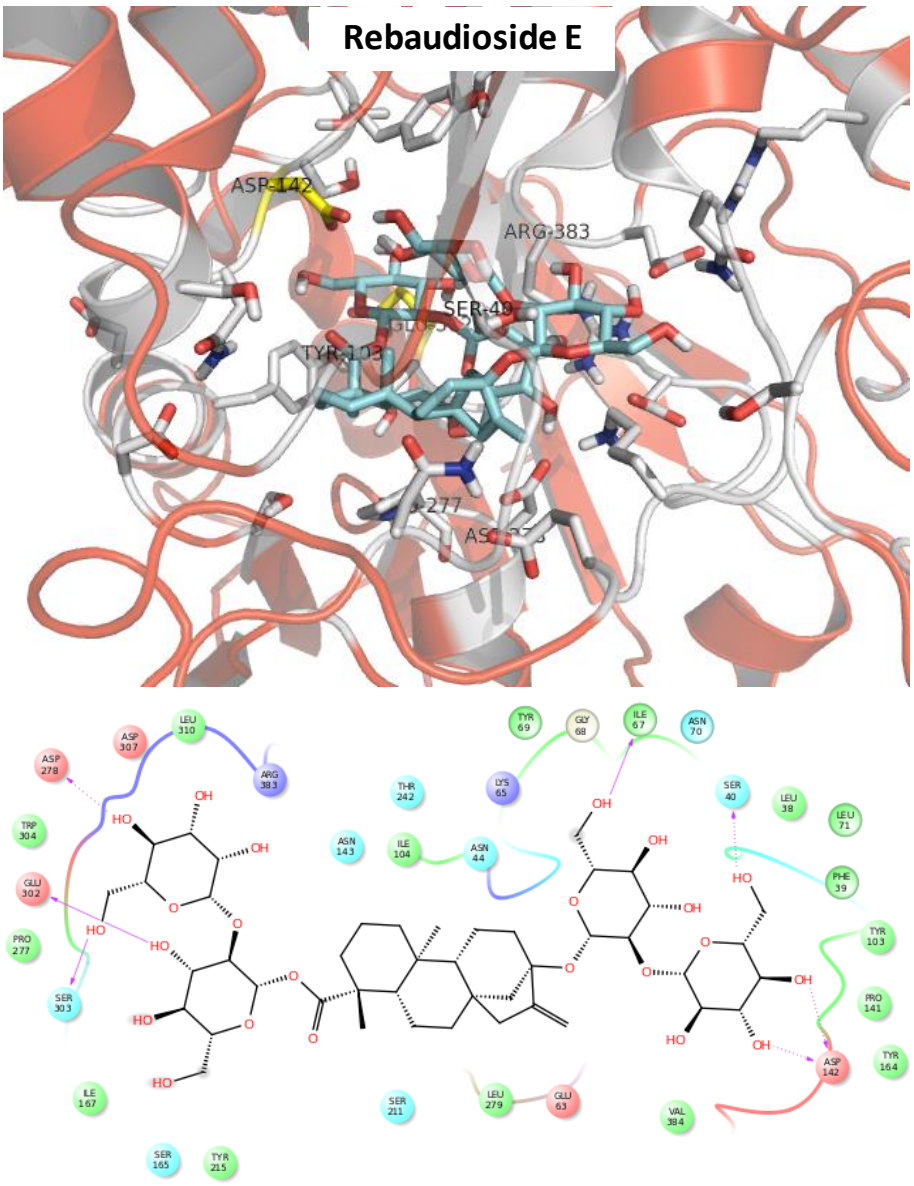
Rebaudioside E
ASP-142
ARG-383
SER-40
TYR-103
-277

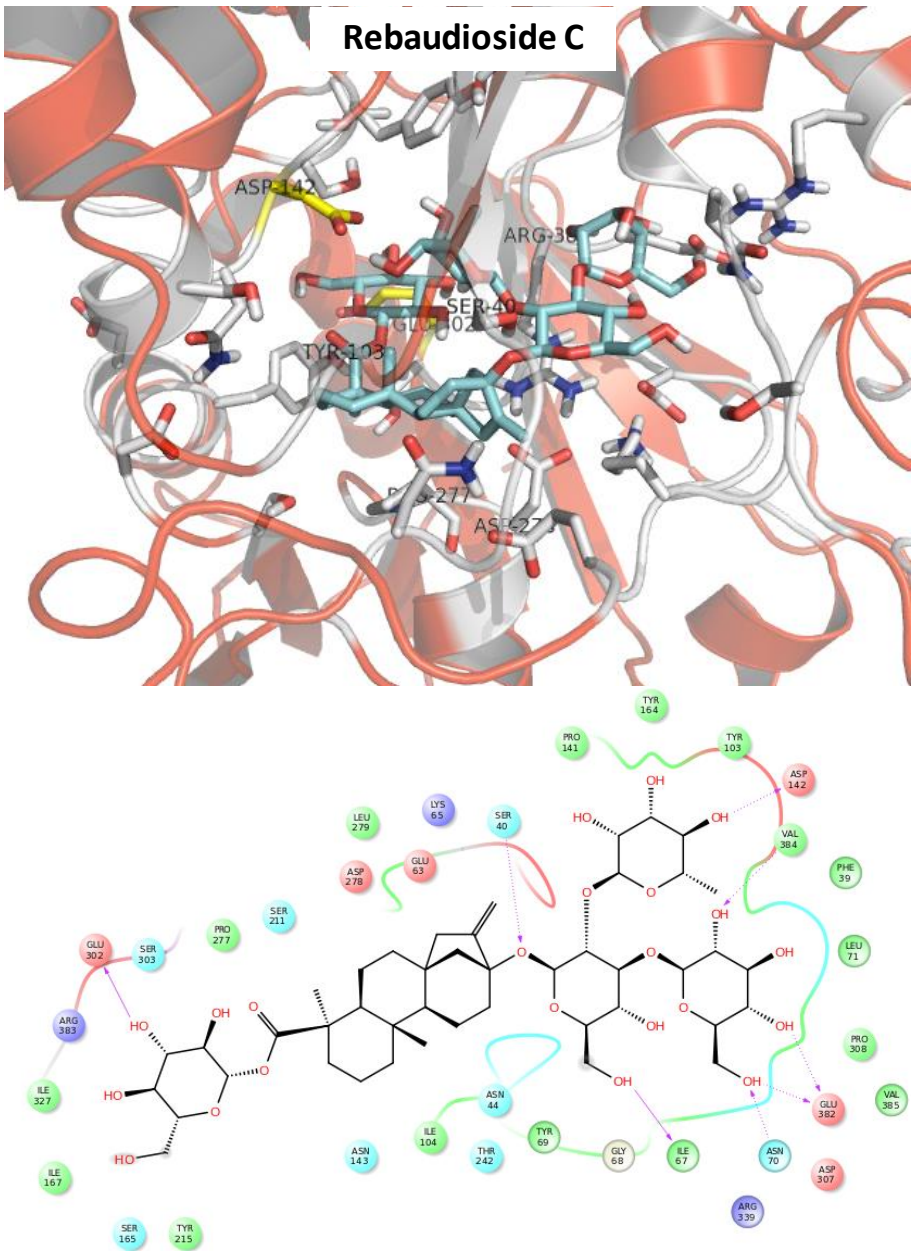
Rebaudioside C
ASP-142
ARG-38
SER-40
TYR-103

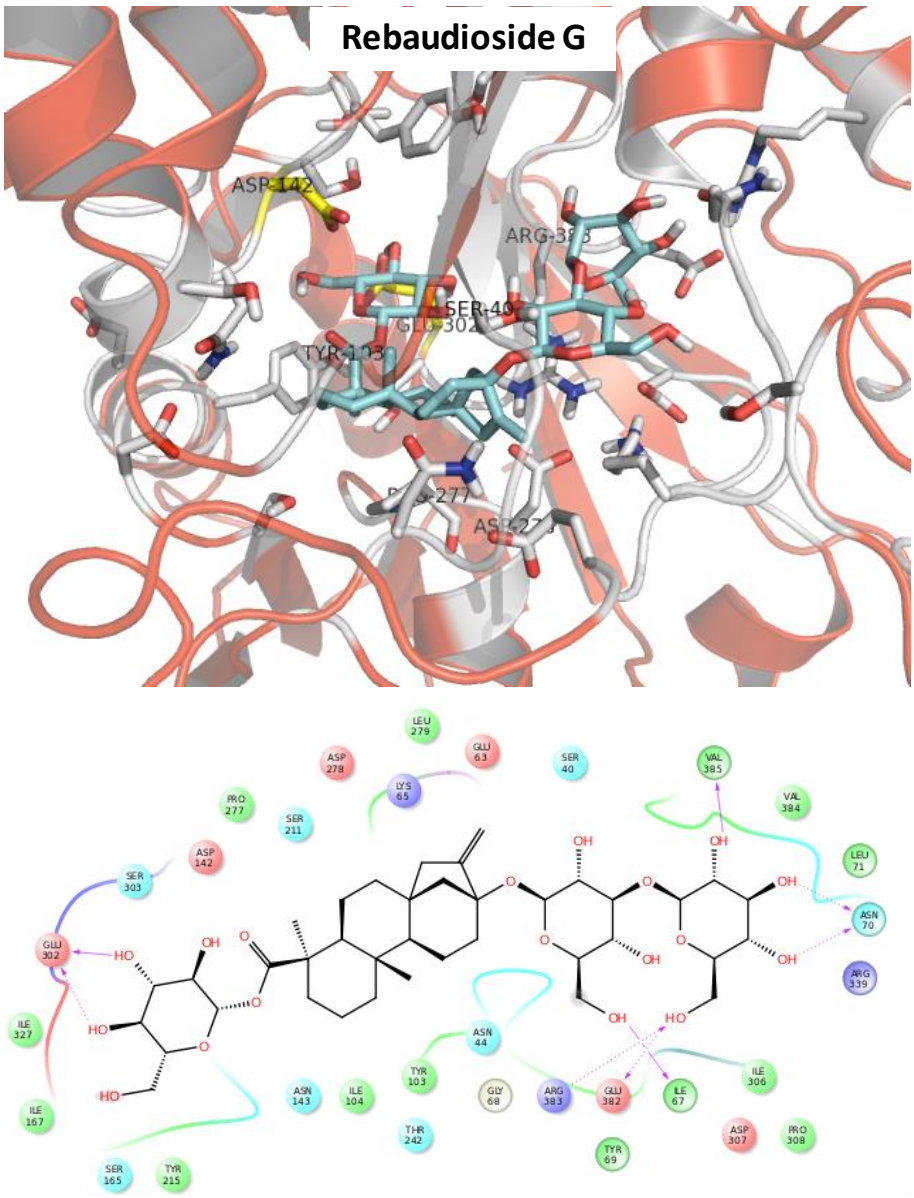

Figure S4. Predicted best binding modes for all sweeteners bound to the Venus flytrap domain (VFD2) of the human sweet taste receptor (TAS1R2/1R3). The predicted pharmacophore is at the bottom. The unified cavity binding components are in **Table S11** of the SI.

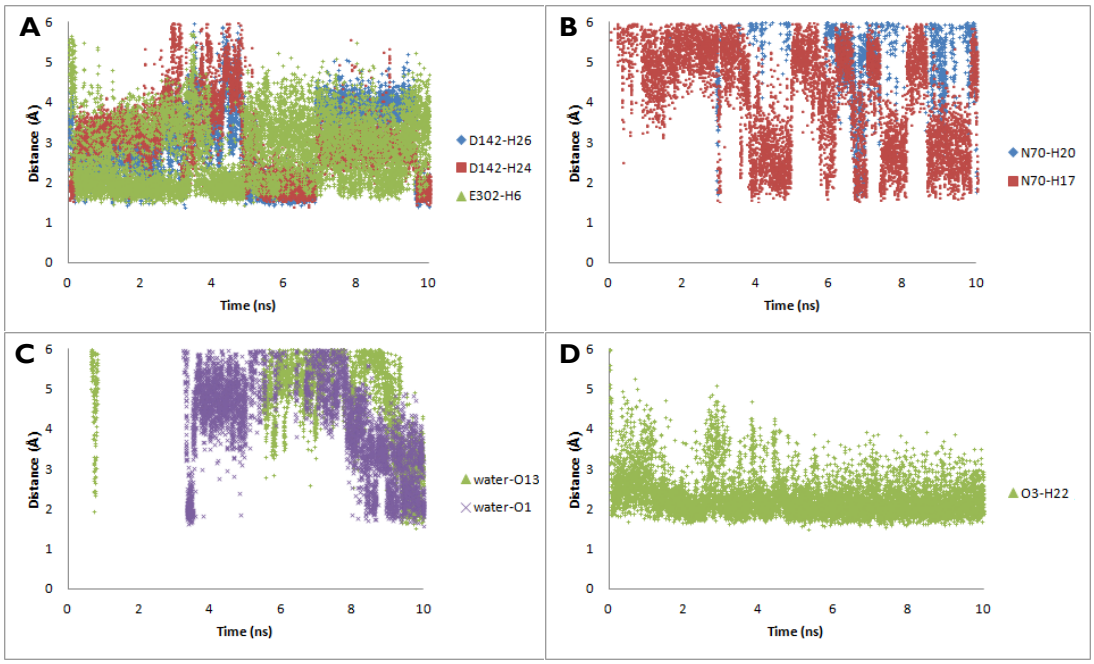

Fig. S5. The trajectory analysis of 10 ns molecular dynamics in the binding site of stevioside at TAS1R2 Venus Flytrap domain.

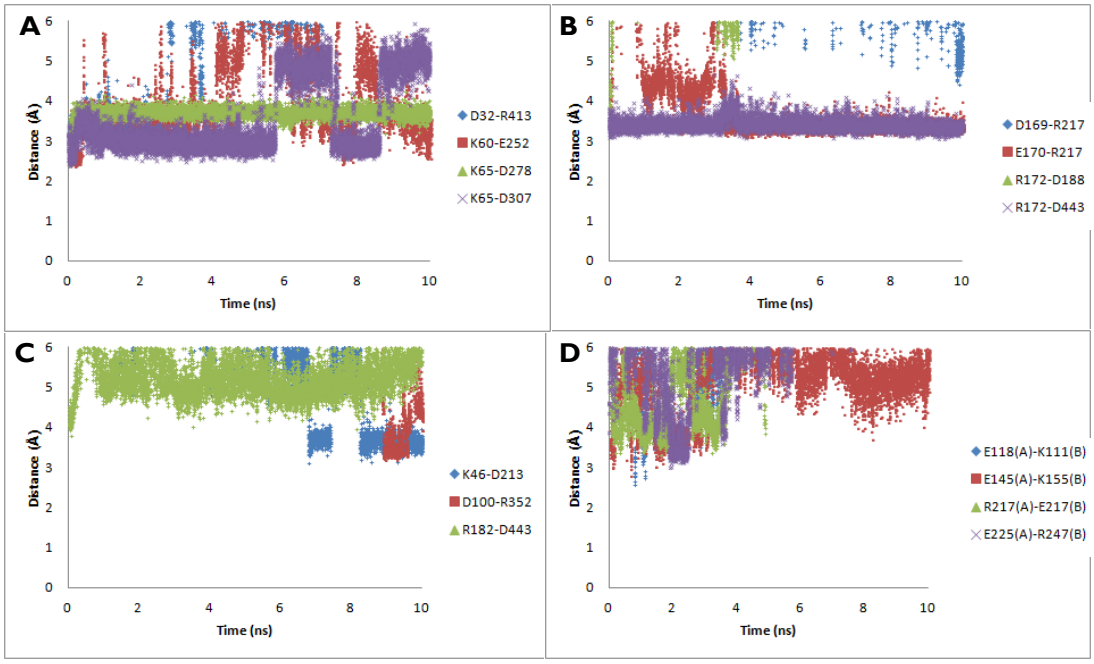

Fig. S6. The trajectory analysis of 10 ns molecular dynamics in the stevioside-bound TAS1R2/ TAS1R3 Venus Flytrap domain.

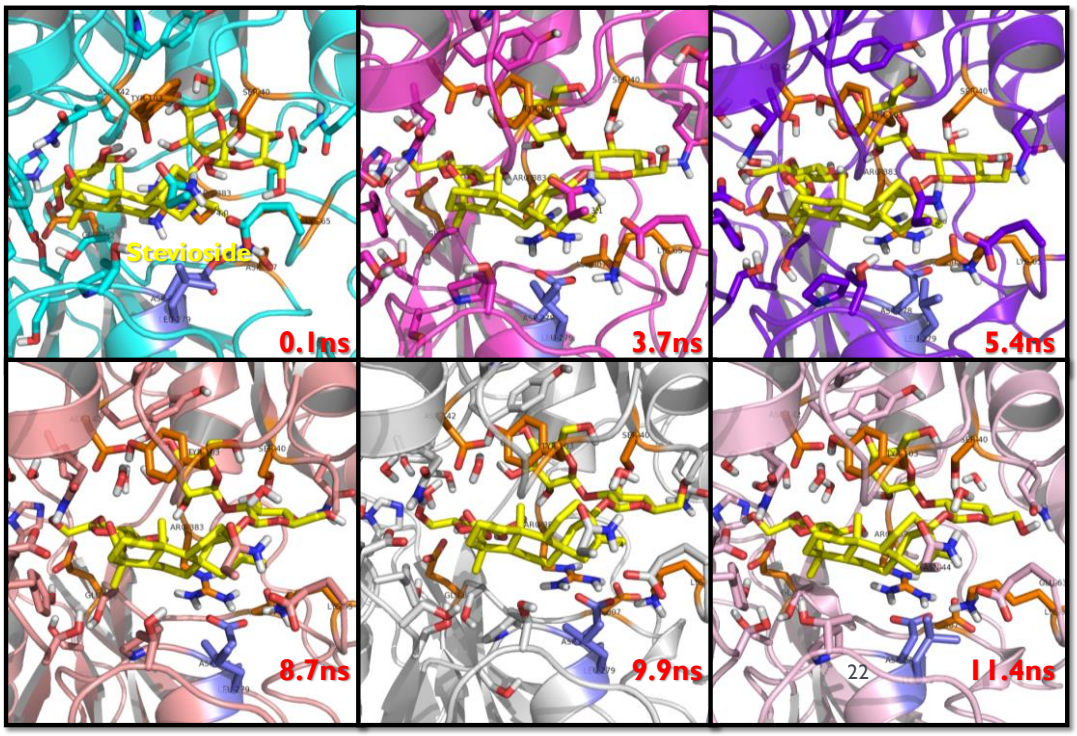

Figure S7. Various snapshots of stevioside bound to the human sweet taste receptor (TAS1R2/ 1R3) Venus Flytrap domains at different time during 12 ns molecular dynamic simulation.

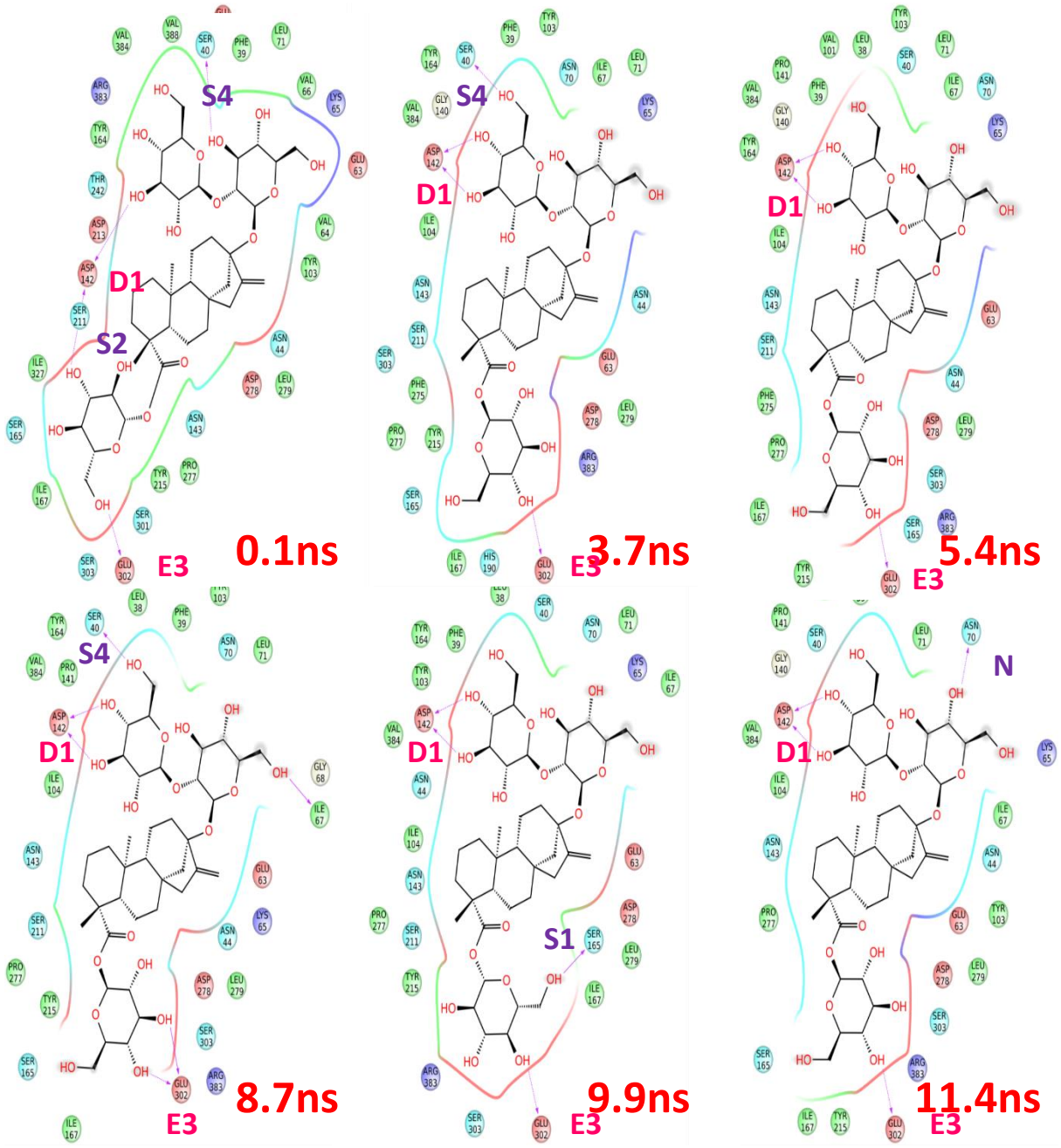

Figure S8. Pharmacophore models for various snapshots of stevioside bound to the human sweet taste receptor (TAS1R2/ 1R3) Venus Flytrap domains at different time during 12 ns molecular dynamic simulation.

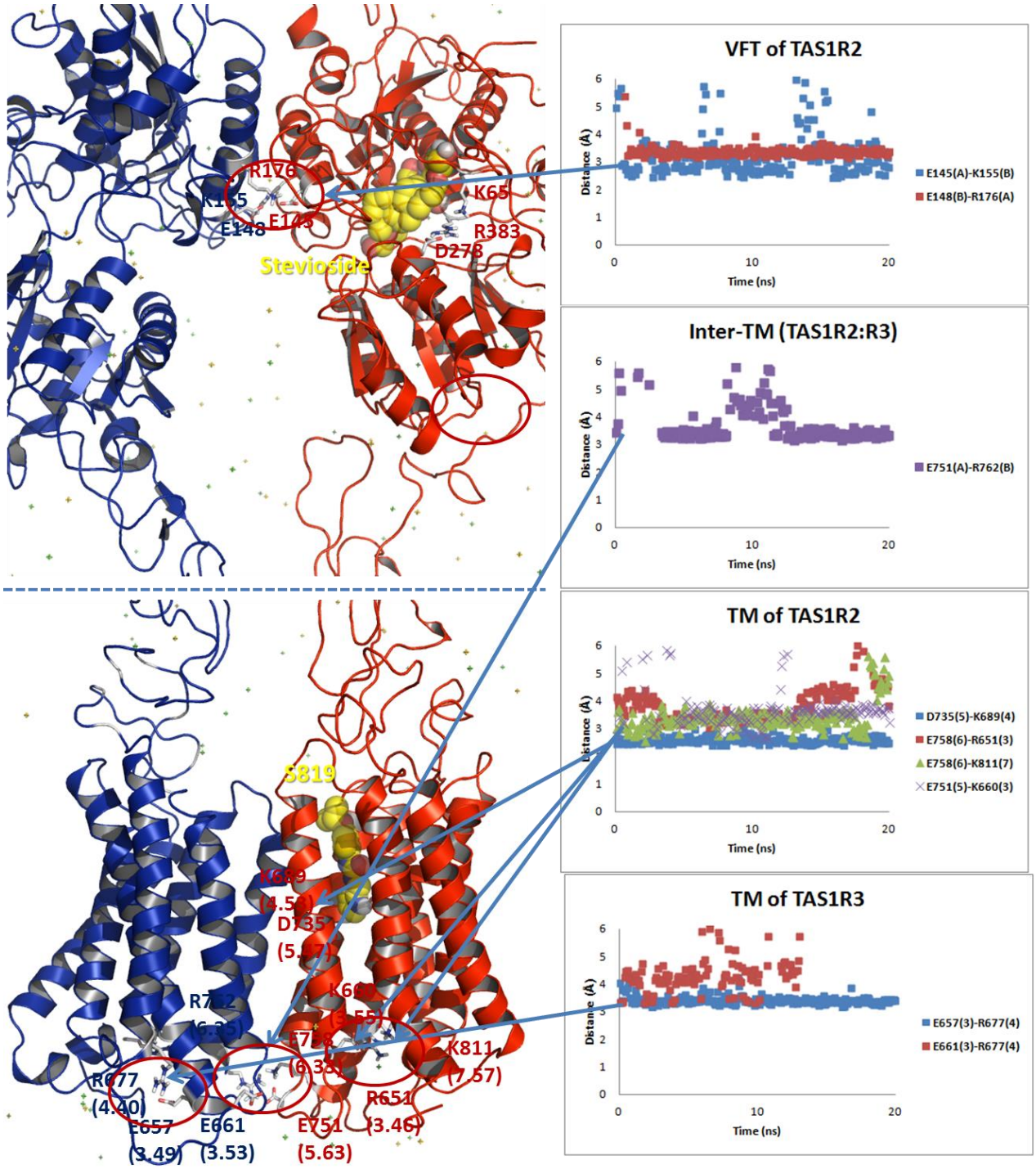

Fig. S9. The trajectory analysis of 20 ns molecular dynamics in the stevioside-S819-bound TAS1R2/ TAS1R3 heterodimer complex including Venus Flytrap domain, cysteine-rich domain and transmembrane domains.

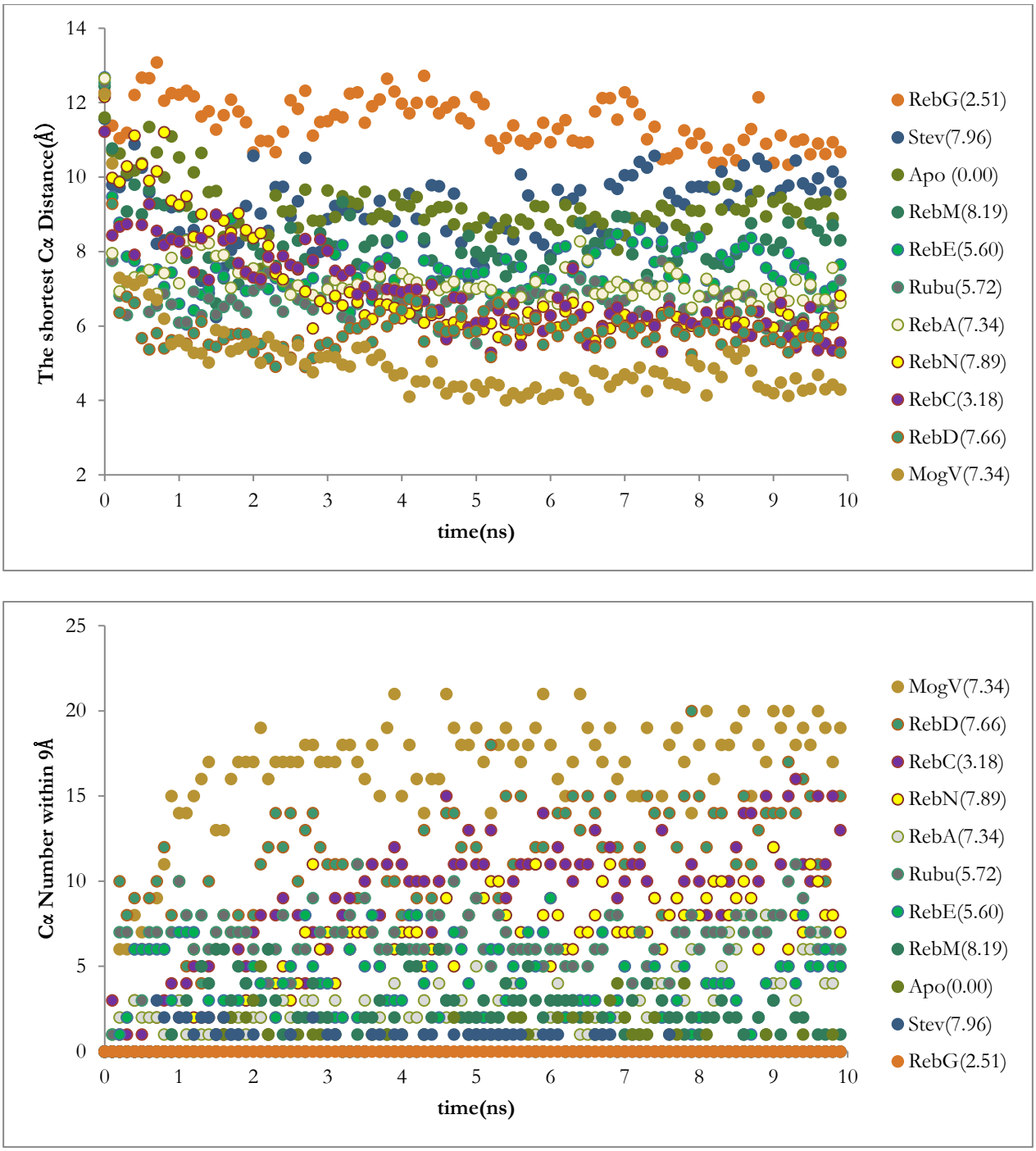

Fig. S10. The shortest TM6-TM6 distance analysis for all 11 ligands and apo protein (top) and the Cα number of TM6-TM6 distances shorter than 9 Å for all 11 ligands and apo protein (bottom)

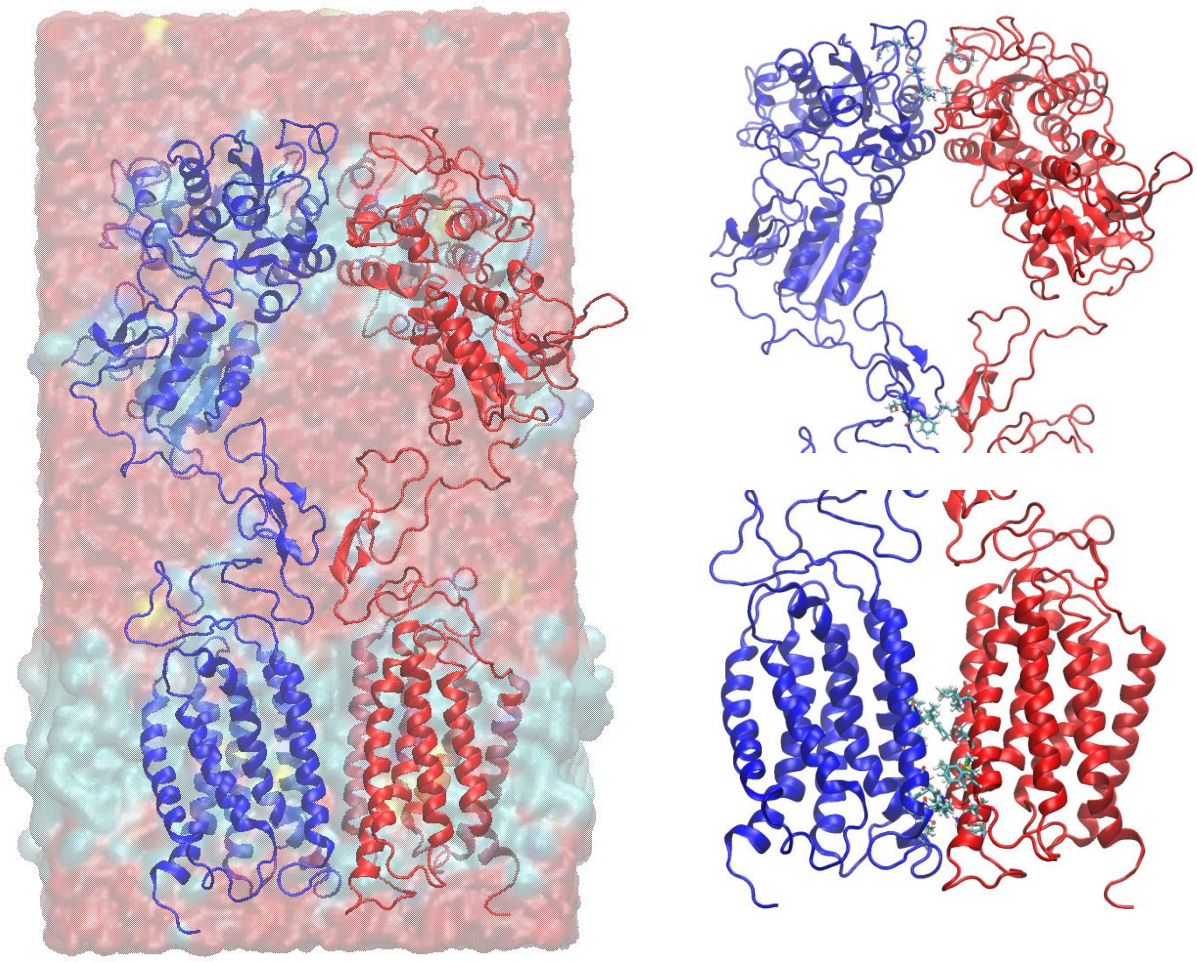

Fig. S11. The average structure of the apo form of the oo-TM4/5 conformation of the sweet receptor. The overall structure is shown in the left panel. The top right panel shows the VFD+CRD regions and the interacting residues between TAS1R2 and TAS1R3 proteins. The bottom right panel shows the TMD region and the interacting residues between TAS1R2 and TAS1R3 proteins. The interacting residues are discussed in the main text.

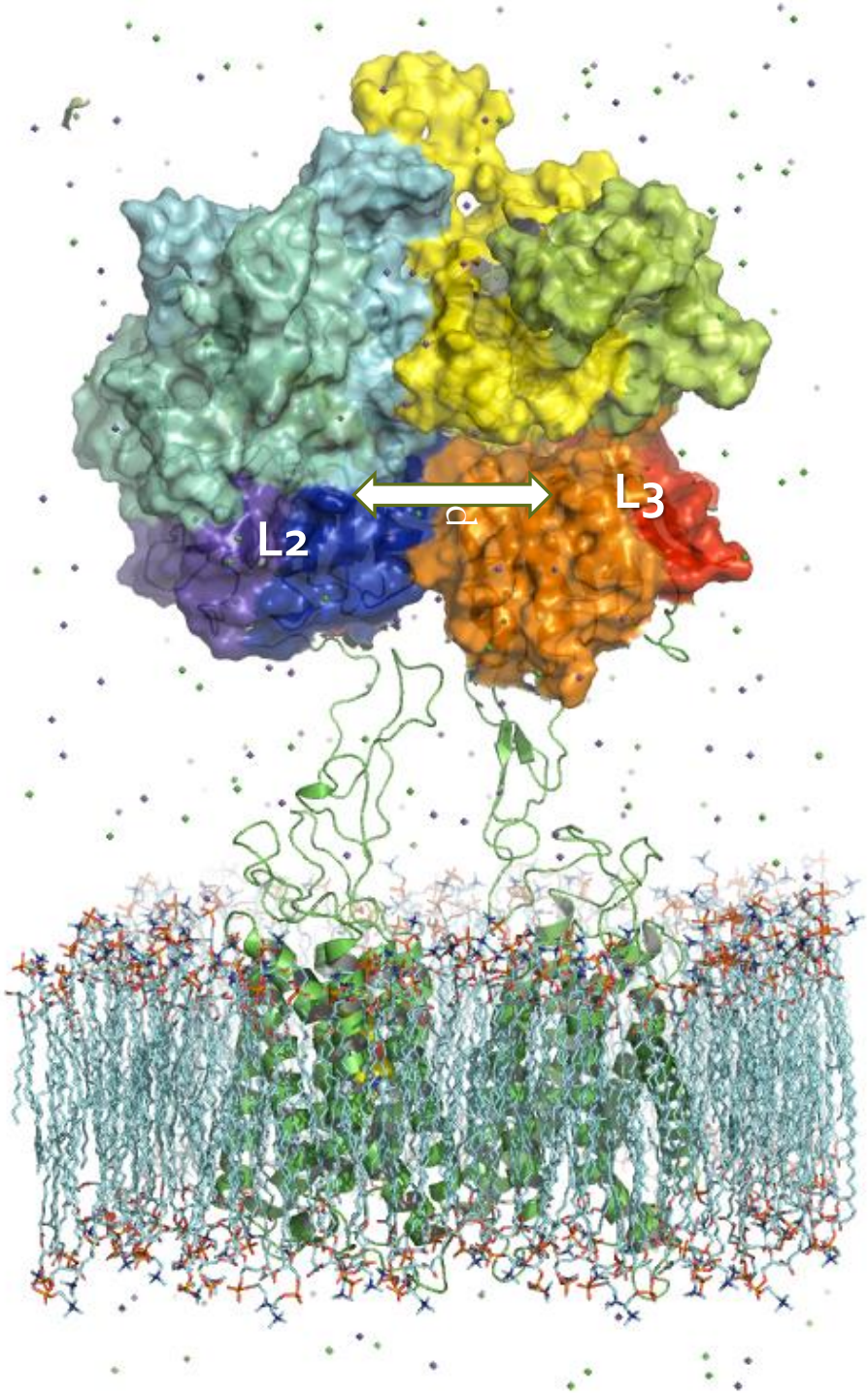

Fig. S12. The definition of the geometric center of two lower Venus Flytrap domain. L2: between 186 - 329 (blue) and 446- 480 (purple) on chain A; L3: between 186 - 329 (orange) and 446 - 480 (red) on chain B.

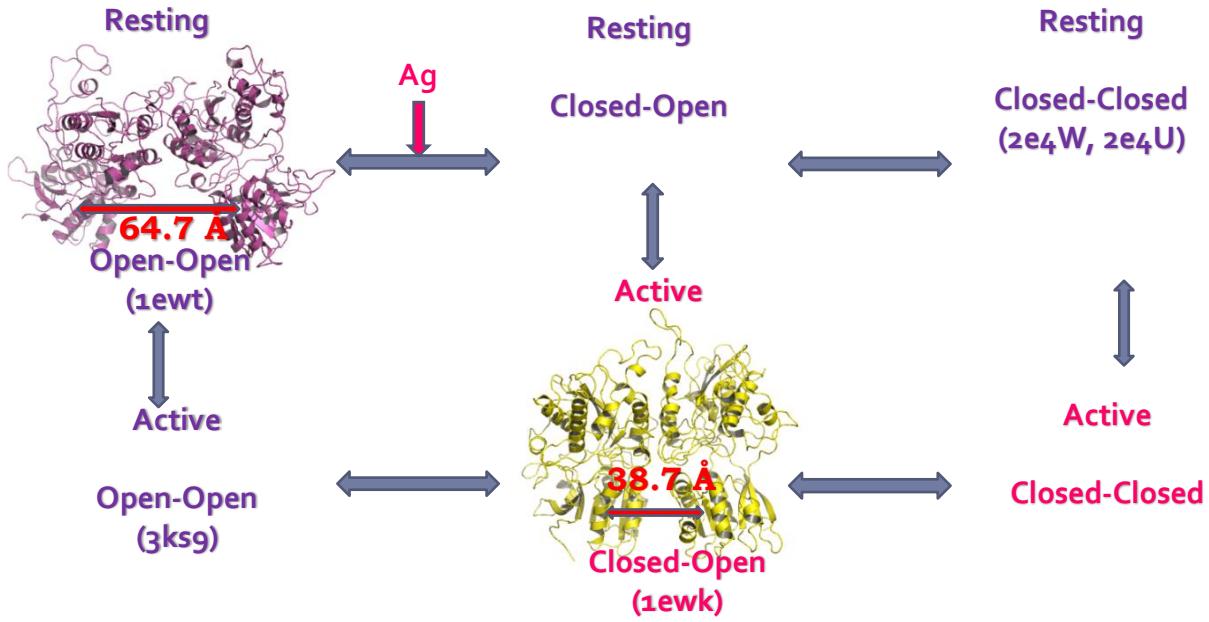

Figure S13. Resting and active structures of the heterodimer TAS1R2/ 1R3 Venus flytrap domains (VFD). The pdb id of crystal structures of metabotropic glutamate receptor are shown in parenthesis.

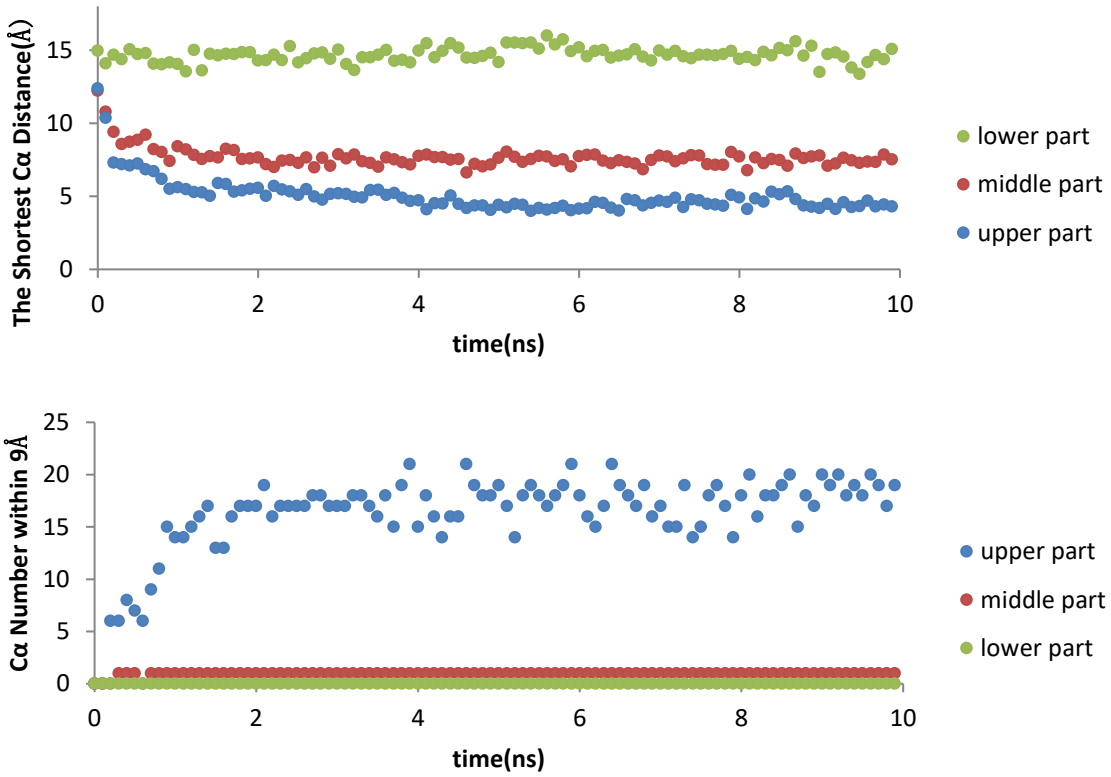

Figure S14. Trajectory analysis of (A) the shortest Cα distance (Top) and (B) Cα number within 9 Å from 10 ns molecular dynamics. Transmembrane 6 (TM6) of sweet taste receptor TAS1R2/ 1R3 was divided into three parts (lower, middle, upper).

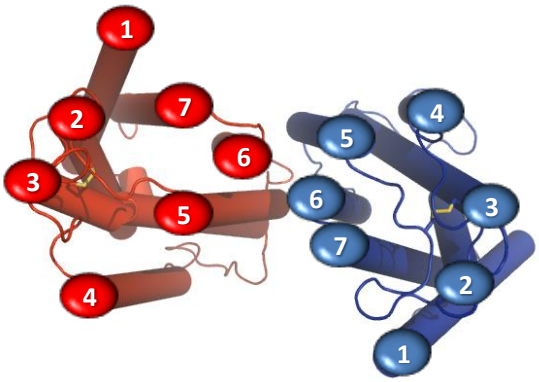

RebM

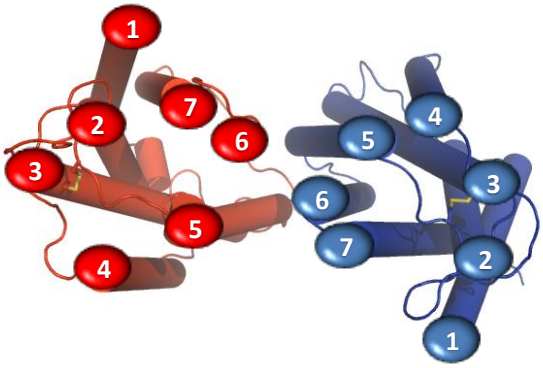

Stev

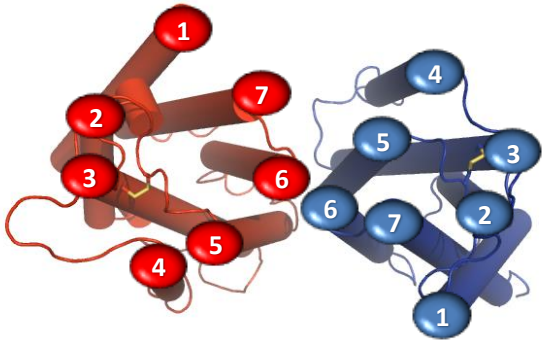

RebN

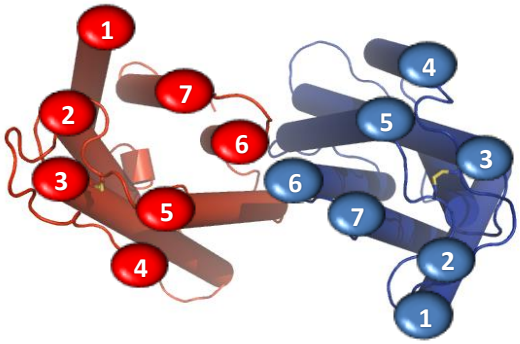

RebD

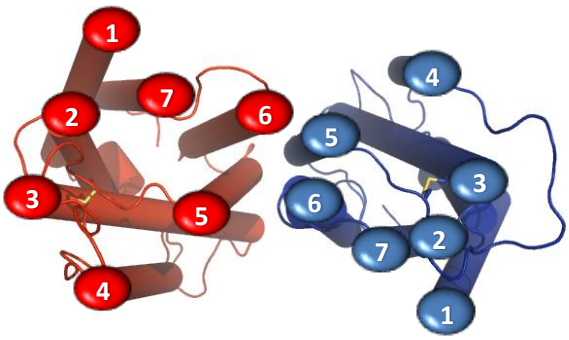

RebA

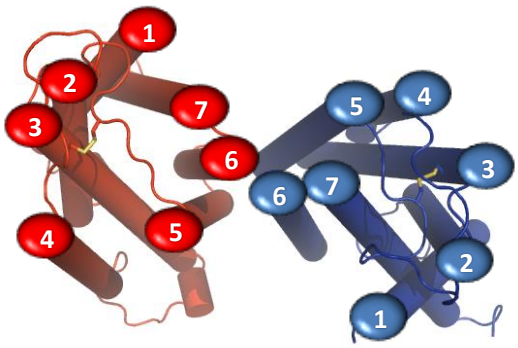

MogV

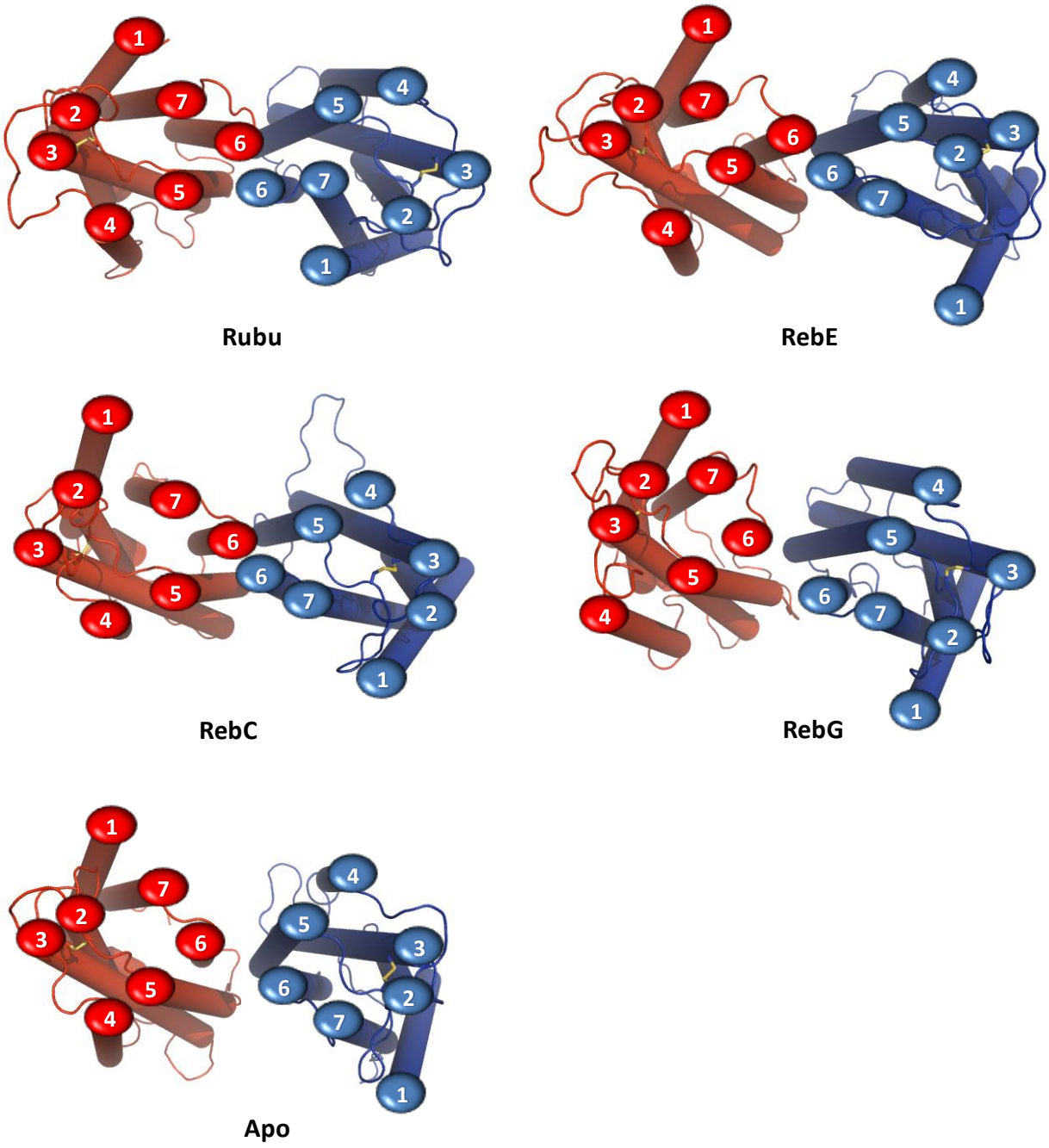

Figure S15. The conformational re-arrangement at the transmembrane domain (TMD) interface of heterodimers of sweet taste receptor TAS1R2 (red)/ TAS1R3 (blue) viewed from the extracellular view after 20ns (310K for 10ns and 400K for 10 to 20 ns) of molecular dynamics.

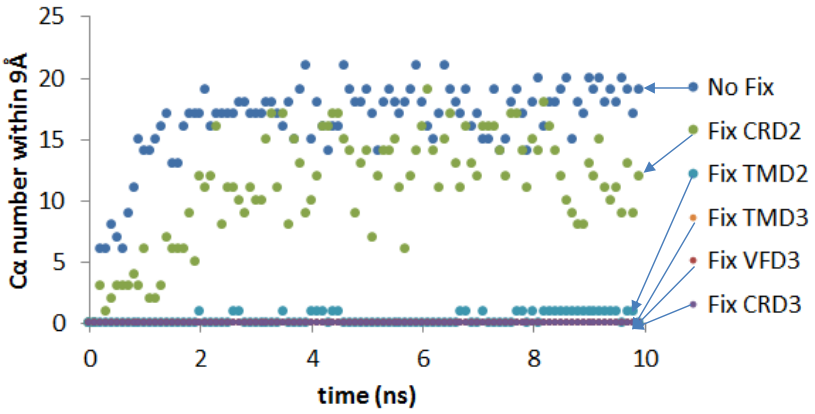

Figure S16. Trajectory analysis of total number Cα between the two TM6s within 9 Å after 10ns of MD.

References

1. Abrol R, *et al.* (2014) Ligand- and mutation-induced conformational selection in the CCR5 chemokine G protein-coupled receptor. *Proc Natl Acad Sci USA* 111:13040-13045.
2. Zhang F, *et al.* (2008) Molecular mechanism for the umami taste synergism. *Proc Natl Acad Sci USA* 105(52):20930-20934.
3. Xu H, *et al.* (2004) Different functional roles of T1R subunits in the heteromeric taste receptors. *Proc Natl Acad Sci USA* 101(39):14258-14263.
4. Jiang P, *et al.* (2005) Lactisole interacts with the transmembrane domains of human T1R3 to inhibit sweet taste. *J Biol Chem.* 280(15):15238-15246.
5. Manglik A, *et al.* (2012) Crystal structure of the μ-opioid receptor bound to a morphinan antagonist. *Nature* 485(7398):321-326.
6. Huang J, Chen S, Zhang JJ, & Huang XY (2013) Crystal structure of oligomeric β1-adrenergic G protein-coupled receptors in ligand-free basal state. *Nat Struct Mol Biol.* 20(4):419-425.
7. Xue L, *et al.* (2015) Major ligand-induced rearrangement of the heptahelical domain interface in a GPCR dimer. *Nat Chem Biol* 11(2):134-140.
8. Hellfritsch C, Brockhoff A, Stähler F, Meyerhof W, & Hofmann T (2012) Human psychometric and taste receptor responses to steviol glycosides. *J Agric Food Chem.* 60(27):6782-6793.
9. Huang S, *et al.* (2011) Interdomain movements in metabotropic glutamate receptor activation. *Proc Natl Acad Sci USA.* 108(37):15480-15485.
10. Hlavackova V, *et al.* (2012) Sequential inter- and intrasubunit rearrangements during activation of dimeric metabotropic glutamate receptor 1. *Sci Signal.* 5(237):ra59.
11. Doumazane E, *et al.* (2013) Illuminating the activation mechanisms and allosteric properties of metabotropic glutamate receptors. *Proc Natl Acad Sci USA.* 110(15):E1416-1425.
12. Abrol R, Bray JK, & Goddard III WA (2011) Bihelix: Towards de novo structure prediction of an ensemble of G-protein coupled receptor conformations. *Proteins* 80:505-518.
13. Wu H, *et al.* (2014) Structure of a class C GPCR metabotropic glutamate receptor 1 bound to an allosteric modulator. *Sci.* 344(6179):58-64.
14. Doré AS, *et al.* (2014) Structure of class C GPCR metabotropic glutamate receptor 5 transmembrane domain. *Nature* 511(7511):557-562.
15. Abrol R, Griffith AR, Bray JK, & Goddard III WA (2012) Structure prediction of G protein-coupled receptors and their ensemble of functionally important conformations. *Methods Mol Biol* 914:237-254.
16. Kunishima N, *et al.* (2000) Structural basis of glutamate recognition by a dimeric metabotropic glutamate receptor. *Nature* 407(6807):971-977.
17. Bordoli L & Schwede T (2012) Automated protein structure modeling with SWISS-MODEL Workspace and the Protein Model Portal. *Methods Mol Biol.* 857:107-136.
18. Wu H, *et al.* (2012) Structure of the human κ-opioid receptor in complex with JDTic. *Nature* 485(7398):327-332.
19. Watts KS, *et al.* (2010) ConfGen: A Conformational Search Method for Efficient Generation of Bioactive Conformers. *J.Chem. Inf. Model.* 50:534-546.
20. Mayo SL, Olafson, B.D., Goddard III, W.A (1990) DREIDING - a generic force field for molecular simulations. *J. Phys. Chem.* 94:8897.

21. Kim S-K, Li Y, Park C, Abrol R, & Goddard III W (2010) Prediction of the 3D structure for the rat urotensin II receptor and comparison of the antagonist binding sites and binding selectivity between human and rat from atomistic simulations. *ChemMedChem* 5:1594-1608.
22. Bhandarkar M, *et al.* (2008) *NAMD User's Guide (Theoretical Biophysics Group, University of Illinois at Urbana-Champaign and Beckman Institute, Urbana)* Version 2.6.
23. Phillips JC, *et al.* (2005) Scalable molecular dynamics with NAMD. *J. Comput. Chem.* 26:1781-1802.
24. MacKerell AD, *et al.* (1998) All-atom empirical potential for molecular modeling and dynamics studies of proteins. *J. Phys. Chem. B* 102:3586-3616.
25. Feller SE, Yin D, Pastor RW, & MacKerell J, A.D. (1997) Molecular Dynamics Simulation of Unsaturated Lipids at Low Hydration: Parametrization and Comparison with Diffraction Studies. *Biophys. J.* 73:2269-2279.